Most Mars minerals in a nutshell: Various alteration phases formed in a single environment in Noctis Labyrinthus

Patrick Thollot, Nicolas Mangold, V. Ansan, Stéphane Le Mouélic, Ralph Milliken, Janice Bishop, Catherine Weitz, Leah Roach, John Mustard, Scott Murchie

▶ **To cite this version:**

Patrick Thollot, Nicolas Mangold, V. Ansan, Stéphane Le Mouélic, Ralph Milliken, et al.. Most Mars minerals in a nutshell: Various alteration phases formed in a single environment in Noctis Labyrinthus. Journal of Geophysical Research. Planets, 2012, 117 (E11), pp.n/a-n/a. 10.1029/2011JE004028 . hal-02305919

HAL Id: hal-02305919
https://hal.science/hal-02305919

Submitted on 4 Jan 2022

HAL is a multi-disciplinary open access archive for the deposit and dissemination of scientific research documents, whether they are published or not. The documents may come from teaching and research institutions in France or abroad, or from public or private research centers.

L'archive ouverte pluridisciplinaire **HAL**, est destinée au dépôt et à la diffusion de documents scientifiques de niveau recherche, publiés ou non, émanant des établissements d'enseignement et de recherche français ou étrangers, des laboratoires publics ou privés.

Copyright

Most Mars minerals in a nutshell: Various alteration phases formed in a single environment in Noctis Labyrinthus

Patrick Thollot,[1] Nicolas Mangold,[1] Véronique Ansan,[1] Stéphane Le Mouélic,[1] Ralph E. Milliken,[2] Janice L. Bishop,[3,4] Catherine M. Weitz,[5] Leah H. Roach,[6] John F. Mustard,[7] and Scott L. Murchie[8]

Received 18 November 2011; revised 9 February 2012; accepted 15 February 2012; published 21 April 2012.

[1] A closed depression in the Noctis Labyrinthus region of Mars (at 10.4°S, 98.6°W), believed to have formed in the Late Hesperian, holds an inner pit partially filled with several hundred meters of stratified material. Compact Reconnaissance Imaging Spectrometer for Mars (CRISM) visible-near infrared reflectance data reveal signatures of numerous hydrated minerals including halloysite/kaolinite, Fe-smectite, Si-OH bearing phases and Fe-sulfates (polyhydrated, monohydrated, and hydroxylated types, including jarosite). We use CRISM data, high resolution imagery (HiRISE) and HRSC (High Resolution Stereo Camera) derived elevation to analyze the morphology, composition and stratigraphy of these materials. We propose an alteration sequence including formation of acid sulfate solutions from groundwater and magmatic sulfur, which then locally altered the basaltic bedrock and layered sediments mainly deposited from volcanic tephra, forming Fe-smectite and Fe-sulfates. The mineral variability can mostly be explained by local variations in the pH of the altering fluids, with original acidity being buffered by dissolution of primary minerals; and by variable fluid input and evaporation and/or freezing rates (resulting in various water/rock ratios). This site shows local formation of almost all classes of minerals identified thus far on Mars without invoking global conditions. Processes related to local volcanic activity and associated hydrothermalism were able to produce, during an era in which the climate is believed to have been cold, a large variety of hydrated minerals. This study highlights the importance of the geological setting of hydrated minerals in the understanding of Mars geologic and climatic evolution.

Citation: Thollot, P., N. Mangold, V. Ansan, S. Le Mouélic, R. E. Milliken, J. L. Bishop, C. M. Weitz, L. H. Roach, J. F. Mustard, and S. L. Murchie (2012), Most Mars minerals in a nutshell: Various alteration phases formed in a single environment in Noctis Labyrinthus, *J. Geophys. Res.*, *117*, E00J06, doi:10.1029/2011JE004028.

1. Introduction

[2] Three main classes of minerals believed to result from aqueous alteration of igneous materials have been identified on Mars from orbit during the past decade (e.g., ferric oxides, namely crystalline hematite [*Christensen et al.*, 2000]; phyllosilicates [*Bibring et al.*, 2005; *Poulet et al.*, 2005]; and sulfates [*Gendrin et al.*, 2005]). Yet, the relative roles of the main geological processes known to have occurred on Mars – volcanic, impact cratering, fluvial, glacial and eolian processes – in the formation of the deposits that contain these minerals remain poorly constrained.

[3] The mineralogical history of Mars that has been inferred recently [e.g., *Bibring et al.*, 2006] envisions an early wetter environment on Mars, either warm or cold, with permanent or transient liquid water on the surface [e.g., *Squyres and Kasting*, 1994; *Gaidos and Marion*, 2003], that favored the formation of phyllosilicates. The environment would then have shifted toward increasing arid and acidic conditions, more favorable to the formation of sulfates. At the end of this purported climate change (3.5/3 Ga), the Martian environment would have become extremely arid, cold and oxidative, and has remained so until today.

[4] In the last few years, other classes of alteration minerals have been identified from orbital data, namely chlorides [*Osterloo et al.*, 2008], opaline silica [*Milliken et al.*, 2008] and carbonates [*Ehlmann et al.*, 2008]. In situ analyses by the MERs (Mars Exploration Rovers) were also

[1]Laboratoire de Planétologie et Géodynamique, CNRS et Université de Nantes, UMR6112, Nantes, France.
[2]Department of Civil Engineering and Geological Sciences, University of Notre Dame, Notre Dame, Indiana, USA.
[3]Carl Sagan Center, SETI Institute, Mountain View, California, USA.
[4]NASA Ames Research Center, Moffett Field, California, USA.
[5]Planetary Science Institute, Tucson, Arizona, USA.
[6]Frontier Technology, Incorporated, Beverly, Massachusetts, USA.
[7]Department of Geological Sciences, Brown University, Providence, Rhode Island, USA.
[8]Johns Hopkins University Applied Physics Laboratory, Laurel, Maryland, USA.

Copyright 2012 by the American Geophysical Union.
0148-0227/12/2011JE004028

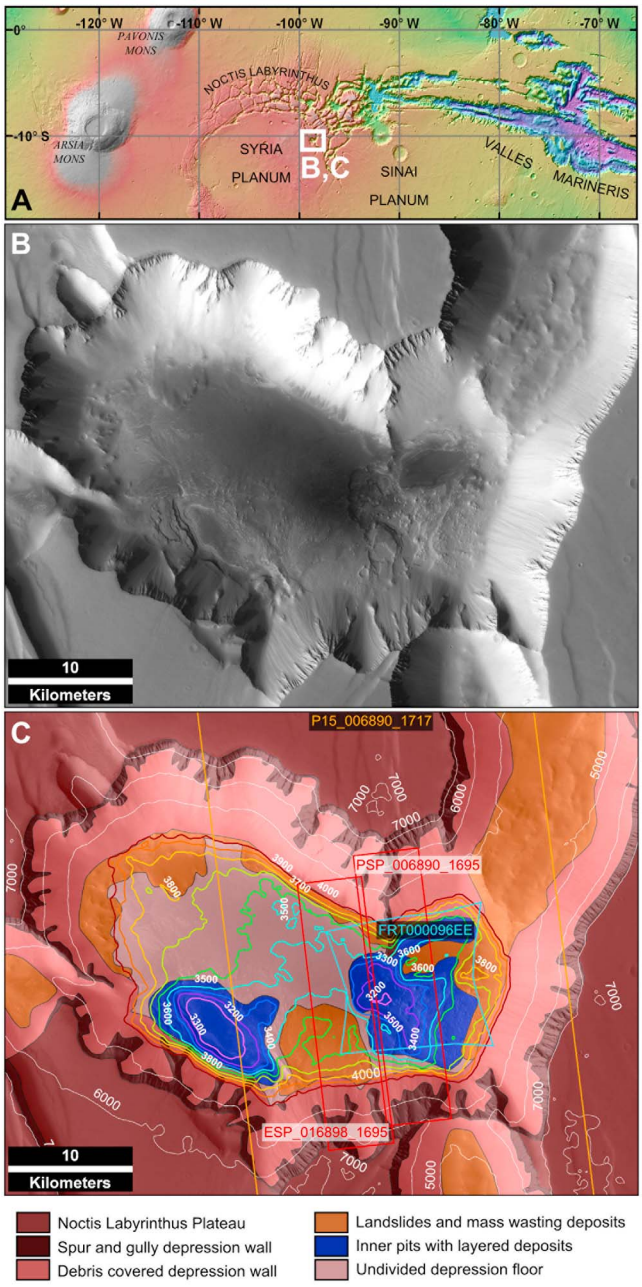

Figure 1. Context of the studied depression. (a) Subset of USGS topographic map of Mars centered on Noctis Labyrinthus. (b) HRSC H1999_0000_ND4 image of the studied depression, centered at (10.4°S, 98.6°W). (c) Same location with geomorphologic map overlain on HRSC image and HRSC DEM (contours with elevation in meters). Orange, red and light-blue outlines show coverage of CTX, HiRISE and CRISM products used, respectively. Product ID's are given on figure.

consistent with the presence of some of these phases (e.g., jarosite and hematite at Meridiani Planum [*Klingelhöfer et al.*, 2004], and in Gusev crater, silica [*Squyres et al.*, 2008; *Morris et al.*, 2008], and carbonate [*Morris et al.*, 2010]). Recently, a classification of deposits bearing hydrated minerals has been proposed [see *Murchie et al.*, 2009b, and references therein], and one type includes interstratified phyllosilicates and sulfates [e.g., *Wray et al.*, 2011]. Also suggested to have been preserved in Gale crater central mound [*Milliken et al.*, 2010], deposits of interstratified phyllosilicates and sulfates are believed to imply repeated changes in geochemical settings during their formation. To sum up, the accumulating evidence show that the history of Mars is not as straightforward as implied by the current paradigm.

[5] With the intent to discriminate between likely formation processes of deposits bearing hydrated minerals, we focus our attention on a site within a depression in Noctis Labyrinthus with some of the greatest mineralogical diversity yet observed on Mars [*Weitz et al.*, 2011]. In this study, we infer that layered deposits in this area have a relatively young age (Late Hesperian or younger) compared to most Martian deposits that contain hydrated minerals, and attempt to constrain the origin(s) of these minerals.

2. Geologic Context

[6] Figure 1 shows the unnamed depression of Noctis Labyinthus (NL) examined in this study, located at (10.4°S, 98.6°W). The depression is one of many in the NL region. Located at the western end of Valles Marineris, NL consists of closed as well as interconnected depressions whose floors occur at various elevations. These NL depressions cut through a plateau mapped as Hesperian-Noachian fractured units of likely basaltic composition. NL is located within a local uplift [e.g., *Masson*, 1980] and may have developed because of regional emplacement and subsequent withdrawal of magmatic reservoirs at a few km depth [*Mège et al.*, 2003]. Increased heat flow associated with magmatic activity could have promoted melting of existing ground ice, in turn promoting creep and slumping of wall material [*Masson*, 1980]. The collapse events that led to the formation of NL depressions have been dated to the Late Hesperian, on the basis of a regional structural study and impact crater densities [*Tanaka and Davis*, 1988], which implies that depressions in NL have offered accommodation space for sediment deposition and accumulation since the Late Hesperian.

[7] NL is located at the center of the Tharsis dome, the largest volcanic province on Mars. Tens of shield volcanoes identified in Syria Planum, 100–400 km away from our study area [*Baptista et al.*, 2008], exemplify ancient local volcanism. Dated to the Late Hesperian, these volcanoes show that nearby volcanic activity was proximal and coeval to the collapse events believed to have formed NL depressions. More recent volcanic activity is indicated by young volcanic plains on the floor of two depressions, identified by *Mangold et al.* [2010a] to the north of NL, and dated to the Late Amazonian. On the edge of one of these plains, *Mangold et al.* [2010b] identified an aqueous alteration layer bearing calcium sulfates or hydrated salts that may be genetically linked to the emplacement of the recent volcanic plains. Together, these observations indicate that volcanism played a role in the evolution of the NL region from the Late Hesperian until the Late Amazonian.

[8] Hydrated phases other than Ca-sulfates and other hydrated salts have been spotted in NL, such as hydrated Si-OH-bearing phases [*Milliken et al.*, 2008] and an unidentified phase [*Roach et al.*, 2010]. More recently, a wide range of hydrous minerals have been identified in

certain depressions within the NL region [*Thollot et al.*, 2010; *Weitz et al.*, 2010]. Specifically, *Weitz et al.* [2011] identified a diversity of minerals (sulfates, clay minerals and hydrated silica) in two depressions in NL, including the one studied here, and proposed varying chemical conditions (aqueous activity and acidity) for their formation.

[9] In this study we build on those initial observations to refine aspects of the stratigraphy, chronology, and formation processes of these deposits, with particular attention to the hydrated minerals. We use available data (spectral, morphological, and topographic) to investigate the bedrock and sedimentary infill of the depression in NL that exhibits the best outcrops and mineralogical signatures. Putting the deposits in their proper geologic context and integrating with knowledge of the conditions necessary to form or preserve the observed minerals, we then propose a scenario for the collective formation and evolution of these deposits that is controlled primarily by local environmental conditions.

3. Data Sets and Methods

[10] We used data sets from Mars Express (MEX) and Mars Reconnaissance Orbiter (MRO). MEX HRSC [*Neukum et al.*, 2004] and MRO Context imager (CTX) [*Malin et al.*, 2007] images were used to build large mosaics at medium spatial resolution (6 to 20 m/pixel). We use MRO High Resolution Imaging Science Experiment (HiRISE) images, with 0.25–1 m/pixel spatial resolution [*McEwen et al.*, 2007], to characterize geological units in detail. All data sets were referenced into a Geographical Information System (GIS) where they could be drawn in the same equidistant cylindrical projection (sphere-based, with a 3396.19 km radius), overlain, and used simultaneously to build a geological map. All the maps shown in this paper are oriented North up.

[11] HRSC data (orbit 1999) were used to provide a Digital Elevation Model (DEM) with a 30 m/pixel spatial grid and ~20 m height accuracy [*Ansan et al.*, 2008]. The DEM was used to determine strike and dip of geologic units at several locations. For each location, several points were fit to a planar layer using ArcGis built-in *trend* routine. This routine returns the three parameters of the Cartesian equation of the plan, and the root-mean square (RMS) error between the data points and the fit. Strike and dip values can then be derived using x and y coefficients. All strikes and dips reported on the map refer to plans with RMS errors between 3 to 15 m, i.e., lower than the DEM vertical accuracy of 20 m, and thus deemed acceptable.

[12] MRO CRISM spectral data were used to infer the mineralogy of the surface material. CRISM [*Murchie et al.*, 2007] is a visible/near-infrared imaging spectrometer with 18 or 36 m spatial and 6.55 nm spectral sampling in targeted mode. We used Full-Resolution-Target (FRT) FRT000096EE cube, which has a 18 m pixel size. CRISM cubes are processed using the CAT (CRISM Analysis Tool) [*Murchie et al.*, 2007] to correct for incidence angle, and to minimize atmospheric contributions using the so-called volcano-scan approach [*Murchie et al.*, 2009c]. We examine data over the Near-InfraRed (NIR) 1–2.6 μm range where many aqueous alteration minerals exhibit diagnostic features. These features are mainly due to absorptions from combinations and overtones of vibrational modes involving oxygen-bearing molecules (mostly water, H_2O), and anions (HO^-, SO_4^{2-}) in coordination with cations (Fe, Mg, Al, Si) [e.g., *Clark et al.*, 1990]. Spectral absorptions investigated here include those related to OH and/or H_2O bearing minerals: the ~1.4 μm band due to the overtone stretching vibrations of metal-OH groups and H_2O, the ~1.9 μm band due to the bending plus stretching combination mode vibration of H_2O [*Cariati et al.*, 1981], and the bands due to the OH stretch plus metal-OH bend combination vibrations at ~2.2 μm (due to Al-OH and Si-OH), ~2.29 μm (Fe-OH), ~2.32 μm (Mg-OH), and at intermediate wavelengths (notably for phyllosilicates with octahedral substitutions) [e.g., *Clark et al.*, 1990; *Bishop et al.*, 2008b]. We also consider absorptions related to OH and SO groups in sulfates at wavelength such as 1.7–1.8 μm, 1.9–2.0 μm, ~2.1 μm, 2.2–2.3 μm and 2.4–2.5 μm [e.g., *Cloutis et al.*, 2006].

[13] We use spectral criteria to build color maps of spectral features with the same approach as *Pelkey et al.* [2007] but we define our own spectral criteria which use medians of several spectral channels to improve the spectral Signal-to-noise ratio (SNR) (Table 1). Mapping spectral criteria translates into generating a composite Red-Green-Blue (RGB) image where the Red, Green and Blue channels each correspond to one criterion. Positive signal from 2 or 3 of the criteria mapped on the same RGB image results in intermediate hues (e.g., positive Red and Blue channels on a pixel make it appear magenta). The criteria maps are built from spectra that have been ratioed to a handpicked spectrally neutral region, on a sample by sample basis (along the same column). This procedure removes column dependent instrumental noise and residual atmospheric effects, also improving the spectral SNR. Individual spectra are checked by hand for variability over individual units. Spectra characteristic of spectrally homogeneous units are averaged over regions of interest of tens to thousands of pixels. These spectra are then compared to library spectra of minerals acquired in the laboratory [e.g., *Clark et al.*, 2007]. We note that apparent absorption bands and spikes at ~1.65 μm in CRISM are artifacts due to the boundary between order sorting filters in the spectrometer [*Murchie et al.*, 2009c]. Based on spectral signatures, we identify mineralogical units. Each unit was named for the mineral that is the most probable match to its spectrum. In non-ratioed CRISM reflectance spectra, diagnostic absorption bands strengths range from 0.3 to 1.3%. These values must be compared with typical absorption band strengths of 10 to 20% in laboratory spectra of pure minerals. A partial dust cover or surficial alteration layer similar to desert varnish on Earth could decrease the strength of absorption bands. Alternatively, the bulk of the units can be made of spectrally neutral primary minerals, which reduce the spectral signatures of hydrated minerals.

[14] For Martian terrains, actual observational constrains on geology are limited by orbital remote sensing techniques at our disposal. NIR spectroscopy only samples the first few tens of microns of surfaces at limited spatial and spectral resolutions. Issues arise concerning the reliability of determination of stratigraphical relationships from images projected on DEM with limited resolutions and spectral identification of mineralogical composition. Most notably, spectral features of each unit are usually pinpointed down to a unique phase, the most spectrally active, even if other

Table 1. Spectral Criteria Used in This Study[a]

Name	Band Center (nm)	Continuum Anchors (nm)	Additional Criteria	Minerals Detected (Non-Exhaustive)
BD1047	1047	1342–2126	-	Fe bearing silicates, sulfates and oxides
BD1922	1922	1862–2080	-	Bound Water in minerals
BD2106	2106	1856–2186	-	Sulfates (Kieserite, Szomolnokite, Romerite)
BD2268	2268	2093–2331	-	Jarosite, Si-OH bearing minerals
BD2285	2285	2245–2338	-	Fe-OH 1:2 Phyllosilicates (Fe smectites)
BD2232	2232	2199–2278	1922 abs. present	Dehydrated Iron sulfates
BD2205L	Sum of: 2146, 2166, 2186, 2205, 2225, 2245, 2265	2113–2338	2205 abs. present & (2166 + 2186) abs. stronger than (2245 + 2265)	Al-OH 1:1 Phyllosilicates (Kaolinite…)
BD2205R	Sum of: 2146, 2166, 2186, 2205, 2225, 2245, 2265	2113–2338	2205 abs. present & (2245 + 2265) abs. stronger than (2166 + 2186)	Si-OH bearing minerals (Opal, hydrated volcanic glass…)
Doublet index	2205 2245 2272	2133–2245 2133–2338 2245–2338	2245 upward feature between 2205 and 2272 must be present; its strength is added to the result	Jarosite, mixtures of Si-OH or Al-OH bearing minerals with Fe smectites…
Fe smectite index	2272, 2291, 2324 2397	2153–2344 2344–2450	2291 abs. must be stronger than 2272 & 2324 abs. & all abs. must be present	Fe-OH 2:1 Phyllosilicates (Fe smectites)
Hydrated salts index	1480 1533 1750 1770 1922 1981 2470	1303–1862 1862–2080 2338–2635	Sums only 1480, 1533, 1750 and 1770 abs. but all 7 abs. must be present	Hydrated salts (polyhydrated sulfates, chlorides…)
Kaolinite index	2172, 2205	2133–2245	Both abs. must be present & 2172 abs. at least 60% of 2205 abs.	Al-OH 1:1 Phyllosilicates (Kaolinite…)
Opal index	2172, 2192, 2212, 2232, 2252, 2272, 2291	2133–2351	Abs. Strength must follow this pattern: 2172 < 2192 < 2212 & 2212 > 2232 > 2252 > 2272 > 2291	Si-OH bearing minerals (Opal, hydrated volcanic glass…)
Sulfate index	1922, 1941, 1981, 2000 2397, 2444	1875–2291 2291–2556	1941, 1981, 2000 abs. must all be stronger than 1922 abs. & all must be present 2397 OR 2444 abs. must be present	Sulfates

[a]All have been customized and are not available in the CAT as distributed by the CRISM team. All band center and continuum anchor values used for criterion computation are taken from the median of values from 3 or 5 spectral channels to increase the signal-to-noise ratio. Note that the criteria bearing a mineral name are just indicative of the mineral they have been designed to pick-up, but not exclusive to this mineral.

minerals are present. We therefore take care in drawing a geological map and inferring stratigraphic sections and cross-sections. One should note that, though built on a careful analysis, these are intrinsically interpretative.

4. Spectral Analysis

[15] HRSC imaging of the studied depression, located at (10.4°S, 98.6°W), is shown in Figure 1b. The depression floor is 3500 m to 3700 m lower than the surrounding Hesperian plateaus. Figure 1c is an interpretative map of this depression. Spur and gully morphology that is common in canyon walls of this region is visible along the upper portions of the depression walls, whereas the lower portions of the walls are covered with talus debris. Part of the depression floor is also covered by debris, which exhibit mounds and blocks tens of meters across, and presumably resulted from mass wasting. Featured in orange in Figure 1c, these debris can be seen notably to the northwest, northeast and south. Two inner pits, featured in blue in Figure 1c, show layered deposits. The layers sit at elevations ranging from ~3200 m to ~3600 m. The surface of the eastern pit is relatively free of dust, suggesting active erosion, while the western pit is covered by a dust blanket obscuring the layers' spectral signature. High-resolution images and spectral data are best exploitable for the eastern pit. Therefore, we then focus our observations on that eastern pit, which we later call simply "pit," on which CRISM data are centered. Its spectral analysis shows a variety of hydrated minerals.

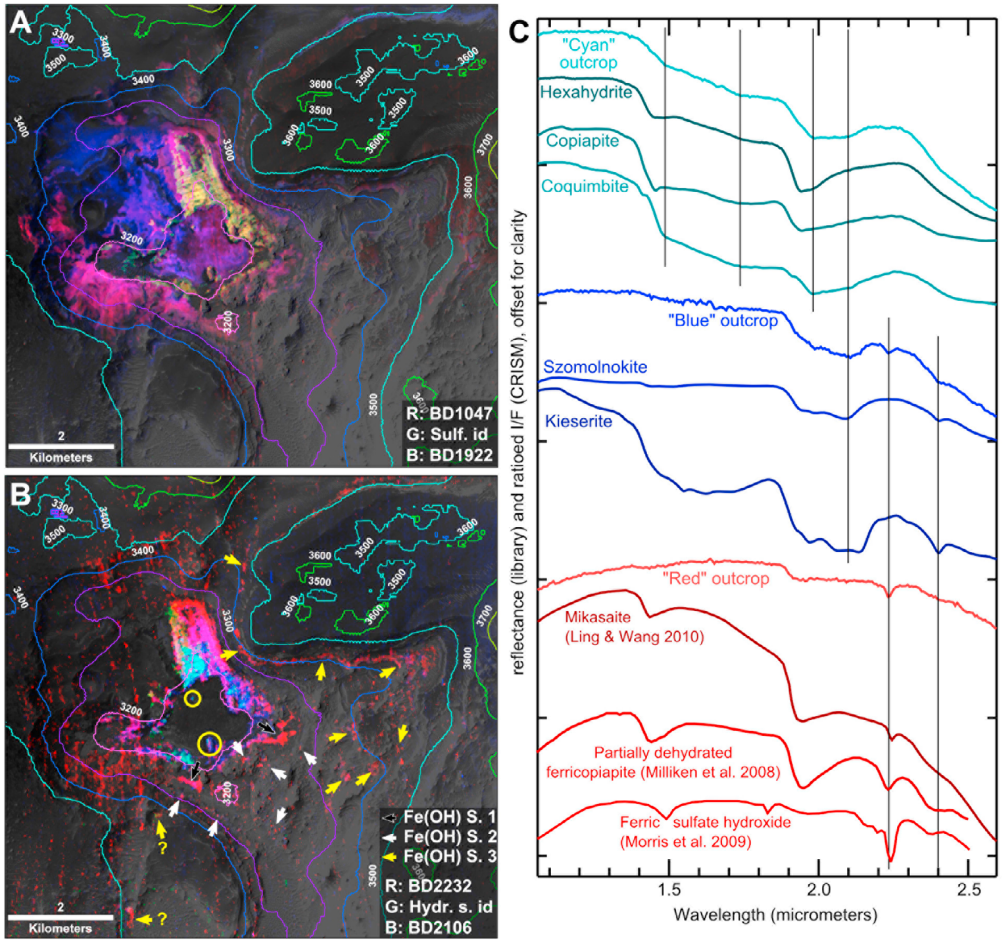

Figure 2. Hydrated minerals, Fe signatures and sulfates. Figures 2a and 2b give RGB composite maps of spectral criteria (defined in Table 1) computed from CRISM FRT000096EE, overlain on CTX image P15_006890_1717. Maps cover the eastern inner pit of the depression located at (10.4°S, 98.6°W) in Noctis Labyrinthus. R, G, B channels set to parameters indicated in lower right corner of the maps. (a) First order spectral characterization of the hydrated minerals in the eastern pit. Fe bearing minerals appear red to magenta, sulfates are greenish and other hydrated phases are blue to magenta. (b) Map of sulfate features. Arrows point to outcrops described in the text (also see caption at lower right corner). (c) Spectra from three different sulfate-bearing outcrops, identified by their apparent color in Figure 2b, compared with library spectra.

4.1. Hydrated, Fe-Rich Minerals and Sulfates

[16] Figure 2a shows the overall occurrence of hydrated minerals in the pit. Spectra from that pit display abundant signatures of hydrated minerals, detectable with the 1.92 μm water absorption band (BD1922 parameter), shown in blue in Figure 2a.

[17] Showing up in reddish tones, widespread $\sim$1 μm Fe absorptions are detected by the drop in reflectance at 1.05 μm (BD1047 parameter). The $\sim$1 μm absorptions are indicative of Fe-rich minerals: Fe oxides/hydroxides/oxihydroxides such as hematite Fe_2O_3 or goethite FeO(OH), Fe-rich sulfates or Fe-rich phyllosilicates. The widespread character of the $\sim$1 μm band may reflect the presence of Fe rich minerals of different types, a contribution from Fe oxides/hydroxides/oxihydroxides on otherwise Fe poor minerals, or a mixture of both. As distinguishing between these hypotheses is challenging, we do not discuss the presence of Fe oxides/hydroxides/oxihydroxides further. However, we note that they may be pervasive over the extent of the pit.

[18] Greenish tones indicate sulfates as detected by the presence of both the 1.9–2.0 μm and $\sim$2.4 μm bands (Sulfate Index parameter): sulfates appear as an almost continuous outline near the 3200 m elevation contour and crop out across $\sim$1 km^2 to the north of the pit. The southeast of the pit is devoid of mineral signatures, which is consistent with an apparent cover of light-toned dust in HRSC and CTX images.

4.2. Sulfate-Bearing Material

[19] Three categories of sulfates can roughly be distinguished spectrally: (1) polyhydrated sulfates (i.e., with more than one water molecule per mineral formula, such as hexahydrite $MgSO_4.6H_2O$) typically feature both 1.9–2.0 μm and 2.4 μm broad bands, (2) monohydrated sulfates (i.e., with one water molecule per mineral formula, such as

kieserite $MgSO_4.H_2O$) usually display a broad ~2.1 μm band, (3) hydroxylated sulfates (i.e., with hydroxyl (OH) but no water in the mineral formula – notwithstanding the presence of water adsorbed on the mineral surface, such as jarosite $KFe_3^{3+}(SO_4)_2(OH)_6$) have distinctive spectra with variable features.

[20] Signatures typical of sulfates have been mapped in Figure 2b: criteria assigned to the red, green and blue channels are respectively proxies for: some hydroxylated sulfates, polyhydrated sulfates, and monohydrated sulfates. Sulfates with various hydration states appear to span a contiguous ~1 km^2 outcrop at elevations ranging from ~3200 m to ~3240 m. Figure 2c shows three average end-member spectra from these outcrops and laboratory spectra for comparison.

[21] Polyhydrated and monohydrated sulfates (showing up in green to blue colors in Figure 2b) outcrop close to the center of the pit, at lower elevations, while hydroxylated sulfates (in red) outcrop at higher elevations. An average spectrum of the most hydrated outcrops, as defined by the highest values of our hydrated sulfate index (Table 1), taken from areas in bright cyan in Figure 2b, is shown as "cyan outcrop" in Figure 2c. It has a general shape consistent with Mg and Fe polyhydrated sulfates. Hexahydrite ($MgSO_4.6H_2O$) is shown as an example of polyhydrated Mg sulfates: these do not fit well the "cyan" outcrop spectrum. Copiapite ($Fe^{II}Fe_4^{III}(SO_4)_6(OH)_2.20H_2O$) and coquimbite ($Fe_{2-x}^{III}Al_x(SO_4)_3.9H_2O$) exemplify polyhydrated Fe-sulfates: the "cyan" outcrop has a spectrum consistent with a large coquimbite component. An average spectrum of an area with a strong value of our criterion for monohydrated sulfates, showing up in blue in Figure 2b, is shown as "blue outcrop" in Figure 2c. This spectrum is consistent with a large szomolnokite ($Fe^{II}SO_4.H_2O$) component, possibly mixed with a small amount of kieserite ($MgSO_4.H_2O$) accounting for the spectral shape longward of 2.10 μm. Another band is clearly visible in the spectrum of this material, at ~2.23 μm. This band is specifically picked up by our BD2232 criterion, shown in red in Figure 2b. An average spectrum of a red outcrop (Figure 2b), with strong 2.23 μm band and no other typical sulfate features, is shown as "red outcrop" in Figure 2c. This spectrum also features a very weak ~1.4 μm OH band and a weak ~1.9 μm water band. *Milliken et al.* [2008] described a similar spectrum from material on the plateau west of Juventae Chasma and matched it with that of a partially dehydrated ferricopiapite obtained from heating of ferricopiapite to 250°C (shown in Figure 2c). *Morris et al.* [2009] also described formation of a ferric sulfate hydroxide bearing a strong 2.23 μm band (see Figure 2c), from dehydration of melanterite ($Fe^{II}SO_4.7H_2O$) at 240°C in air (while ferrous szomolnokite formed by dehydration at lower temperature or in dry N_2). This material then has been identified in Aram Chaos by *Lichtenberg et al.* [2010] and in Ophir Chasma by *Wendt et al.* [2011]. *Bishop et al.* [2009] also discussed formation of material with the same 2.23 μm band from various hydrated Fe-sulfates (including copiapite, szomolnokite and hydronium jarosite) and attributed that band to Fe-OH in hydroxylated ferric sulfates. Finally, *Ling and Wang* [2010] acquired the spectrum of material that was formed by heating of amorphous hydrated Fe-sulfate (shown in Figure 2c), also showing a ~2.23–2.24 μm band. Their attribution of this spectrum to mikasaite, an anhydrous ferric sulfate ($Fe_2^{III}(SO_4)_3$), is questionable due to ~1.4 μm OH and ~1.9 μm water bands, indicating persistence of some water. In fact, the 2.23 μm band, at the position expected for metal-OH absorptions, likely reveals formation of a hydroxylated Fe-sulfate. Considering published laboratory constraints and discussions, and considering the association of the 2.23 μm band bearing material we observe with polyhydrated and monohydrated Fe-sulfates, we attribute the 2.23 μm band to hydroxylated Fe-sulfate phases, possibly formed by dehydration of hydrated Fe-sulfates. We then call these phases "Fe(OH) sulfates."

[22] The observed Fe(OH) sulfates occur as mixtures with hydrated sulfates, as evidenced by the 2.23 μm band in the "blue" outcrop spectrum in Figure 2c, or in individual layers. Some outcrops with Fe(OH) sulfates spectral signatures are distinct from the main unit and are pointed by arrows on Figure 2b: black arrows ("Fe(OH) S. 1") show outcrops at ~3240 m, in possible continuity with the main unit; white arrows ("Fe(OH) S. 2") show small patches cropping out at ~3260 m, possible remnants of another layer; yellow arrows ("Fe(OH) S. 3") indicate a unique step-forming layer at ~3400 m. Yellow arrows labeled with a question mark indicate a possible analog to this last layer to the south of the pit, also step-forming and at comparable elevation, with spectral signatures consistent with Fe(OH) sulfates and jarosite components. Jarosite, a specific hydroxylated Fe-sulfate, has been identified in mixtures with phyllosilicates and Si-OH bearing materials and its detection will thus be discussed later.

[23] The Fe-sulfates observed have different hydration states while current Mars surface conditions, being extremely arid, could favor complete dehydration of hydrated Fe-sulfates, which would challenge our identifications. *Wang and Ling* [2011] investigated experimentally the stability and dehydration of ferricopiapite ($Fe_{2/3}^{III}Fe_4^{III}(SO_4)_6(OH)_2.20H_2O$), one of the most hydrated Fe-sulfate minerals. They found that ferricopiapite, though dehydrating in air at temperatures above 5°C (in over a year at 21°C), remains stable for at least 3 years at low temperature (5 to −10°C), even down to 11% relative humidity. Even in mars-like water vapor pressure (~0.09 Pa), and at room temperature, dehydration of ferricopiapite reached a limit after loss of 6 water molecules per mineral formula. They also showed that hydrated sulfates are good buffers for high relative humidity and concluded that dehydration of sulfates on Mars would be avoided just under the surface exposed to arid conditions. As suggested by these experiments, dehydration of Fe-sulfates when exposed at the surface of Mars could take on the order of years, or more. We thus consider that the variability observed in Fe-sulfate (de)hydration could result from different ages of exposition at current surface conditions.

[24] Layered Fe-sulfate bearing units will later be named according to the hydration state of the Fe-sulfates: Layered Sulfates Hydrated (LSH) for polyhydrated Fe-sulfates and Layered Sulfates Dehydrated (LSD) for monohydrated and hydroxylated Fe-sulfates.

4.3. Hydrated Phyllosilicates

[25] Hydrated phyllosilicates can be identified spectrally by the combination of the narrow ~1.4 μm and 1.9 μm bands of water with various metal-OH bands in the 2.2–2.3 μm range [see *Bishop et al.*, 2008b, and references therein]. Kaolinite group Al-phyllosilicates, such as

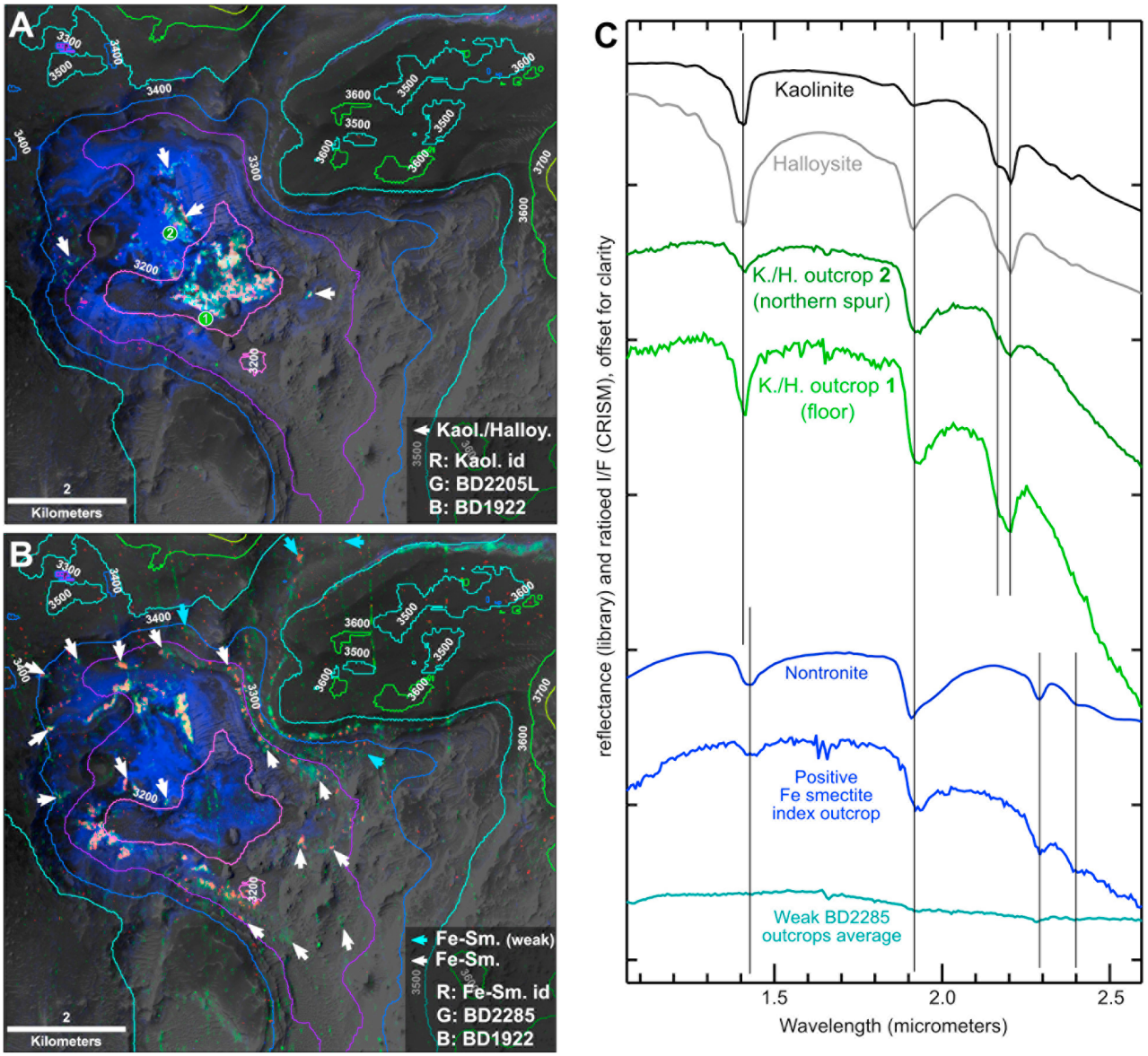

Figure 3. Hydrated phyllosilicates. Figures 3a and 3b give RGB composite maps of spectral criteria (source data: see Figure 2). R, G, B channels set to parameters indicated in lower right corner of the maps. Arrows point to outcrops described in the text (also see caption at lower right corner). (a) Map of kaolinite group mineral features. (b) Map of Fe-smectite features. (c) Spectra from two kaolinite/halloysite bearing outcrops (in green), identified by circled numbers in Figure 3a, and from two Fe-smectite bearing outcrops (blue and cyan), compared with library spectra.

kaolinite and halloysite, feature an asymmetric Al-OH band at and shortward of ~2.21 μm, picked up by our criteria "BD2205L" and "kaolinite index" (Kaol. Id, more specific to the exact band shape). Fe-smectites feature a Fe_2-OH band at 2.29 μm and a weaker ~2.4 μm band. Our BD2285 criterion picks up the 2.29 μm band while our Fe-smectite index picks up both. Maps of spectral criteria for kaolinite group phyllosilicates and Fe-smectites are shown on Figures 3a and 3b, respectively.

4.3.1. Halloysite

[26] The largest outcrop of material bearing kaolinite-like signatures, spanning ~1 km^2, sits at the lowest elevations in the pit (~3200 m). The same material also crops out to the west, up to 3350 m, and at the surface of a low spur, extending to the north up to 3250 m. An outlier is visible to the east at ~3220 m. Figure 3c shows average spectra from two major outcrops: spectral features fit well those for the hydrated analog to kaolinite, halloysite-10Å ($Al_2Si_2O_5(OH)_4.2H_2O$), also referred to as "endeillite" or "hydrated halloysite" in the literature.

[27] The identification of halloysite or kaolinite associated with Fe-sulfates, like coquimbite, is surprising as the latter precipitate at pH < 1 or less, i.e., well below the admitted stability field of halloysite. *Altheide et al.* [2010] studied experimentally the dissolution of kaolinite and found that it kept its characteristic spectral signature when treated with

acid sulfate solutions of pH down to 2. In pH ~ 0 solution, kaolinite did lose its spectral signature but the bulk remained intact according to XRD analysis. Thus, natural kaolinite/halloysite altered by acid solutions down to pH ~ 0 but then partly eroded would still have a characteristic spectral signature. Active erosion is also consistent with the presence of halloysite signatures, despite its instability under the dry Martian surface conditions [*Joussein et al.*, 2005].

[28] Alternatively this material could be a mixture of kaolinite with other hydrated phases. For instance, *Clark et al.* [1990] prepared a 75:25 physical mixture of kaolinite: montmorillonite which had a spectrum very similar to that of pure halloysite. A recent study by *McKeown et al.* [2011] on Al-clays intimate mixtures shows that mixtures of kaolinite with up to 50% montmorillonite could also fit the observed halloysite-like spectra. We then define a corresponding unit, simply named "H" for halloysite.

4.3.2. Fe-Smectite

[29] The largest outcrop of Fe-smectite rich material, to the north of the deepest area of the pit, overlies sulfate-bearing material from ~3230 m upward. The spectrum from this area matches that of nontronite, a Fe-smectite of ideal formula $(Na_{0.3})Fe^{III}_2(Si,Al)_4O_{10}(OH)_2.nH_2O$, as shown in Figure 3c. Spectra from areas pointed by white arrows in Figure 3b show very similar spectra, and outcrop at elevations from ~3230 m to ~3300 m. Cyan arrows pinpoint low 2.285 μm absorptions at higher elevations, around ~3400 m. Averaging thousands of pixels at similar elevation and with similar albedo around these locations yields a spectrum with weak features consistent with a Fe-smectite component (cyan spectrum in Figure 3c) and a contribution of clinopyroxene (very broad 1 and 2.2 μm bands), probably in the form of a sand cover. We therefore distinguish a "lower" Fe-smectite unit with strong signatures, later named "LSm1" (Layered Smectite 1) and an "upper" Fe-smectite unit with weaker signatures, later named "LSm2" (Layered Smectite 2).

4.4. Si-OH-Bearing Material

[30] Figure 4a is a map of spectral features characteristic of Si-OH bearing material (including opaline silica), including a diagnostic asymmetric 2.21 μm absorption band [e.g., *Milliken et al.*, 2008]. Our criteria for this material (Opal Index and BD2205R) pick up two outcrop clusters located to the north and southwest of the pit, at elevations ranging from ~3250 m to ~3500 m. This material is in contact with Fe-smectite-bearing material at several elevations (red arrows in Figure 4a, e.g., ~3250 m and ~3300 m to the north and south, ~3400 m to the west).

[31] Figure 4c shows in red as "outcrop 1 (positive opal id)" an average spectrum from the southwestern yellowish areas of Figure 4a. This spectrum has a diagnostic asymmetric ~2.2 μm absorption band leaning toward long wavelengths. Locally, spectra from positive opal id outcrops show some variability from this typical broad 2.2 μm band, including a dip at 2.17–2.20 μm (absorption found in halloysite), a dip at 2.29 μm (like from Fe-smectite), and a dip at 2.23 μm (Fe-sulfate). This variability suggests intimate and/or spatial mixture of several minerals in some places. In addition, the positive opal id material likely bears Fe-oxides/hydroxides/oxihydroxides, as shown by the positive BD1047 parameter at the same locations (compare Figure 2a with Figure 4a). The ~1.4 μm band of positive opal id material varies locally in width and position from a narrow band centered at ~1.38 μm to a broad band centered at 1.40 or 1.41 μm. Along with the positive opal id average spectrum, spectra of reference materials are shown in red in Figure 4c.

[32] Opal-A/CT exemplifies opaline material such as hydrated silica and opal. Opal-A/CT has an asymmetric 2.21 μm absorption that extends longward toward ~2.26 μm, forming a 2.21–2.26 μm plateau that does not match that of the positive opal id material spectrum. Studies of Si-OH bands in spectra of opal, hydrated silica gel and opaline silica on altered glass [e.g., *Anderson and Wickersheim*, 1964; *Swayze et al.*, 2007; *Milliken et al.*, 2008] have shown that the Si-OH stretching overtone occurs near 1.38 μm for dehydrated Si-OH bearing phases and that this band broadens and shifts toward 1.41 μm as H-bonding of water molecules to Si-OH groups increases with the addition of water. Similarly the 2.21–2.26 μm band of opal-CT sharpens and shifts toward 2.20 μm with dehydration. On the contrary, unaltered hydrated glasses with various amounts of water in the structure all feature a broad band centered at 2.23 μm (*Milliken et al.* [2008]; see online GSA Data Repository item 2008220, available at http://www.geosociety.org/pubs/ft2008.htm). The positive opal id material is consistent with low crystallinity and low hydration hydrated silica.

[33] A spectrum of a lapilli from Hekla is shown as an example of unaltered volcanic glass. A sample of lapilli from Hekla in Iceland was heated for 24 h at 110°C to remove adsorbed water and a spectrum was acquired with a Nicolet 5700 Fourier Transform Infrared Spectrometer. The Hekla lapilli consists of unaltered or barely altered light-toned volcanic glass. XRD analysis showed that the sample was amorphous with no detectable mineral phase and a broad hump from $2\Theta \sim 15°$ to ~30° consistent with amorphous silica. The spectrum of the Hekla lapilli has a sharp 1.41 μm band and a broad ~2.23 μm asymmetric absorption similar in shape to that of the positive opal id material, but at slightly longer wavelength, consistent with spectra of synthetic unaltered hydrated basaltic glasses acquired by *Milliken et al.* [2008] and not consistent with the positive opal id material.

[34] Montmorillonite is an Al-rich 2:1 phyllosilicate of ideal formula $(Na,Ca)_{0,3}(Al,Mg)_2Si_4O_{10}(OH)_2.n(H_2O)$ of which spectra have a 2.21 μm absorption due to Al-OH groups. The montmorillonite Al-OH absorption is symmetric and does not show the asymmetry of the 2.2 μm band of the positive opal id material. In addition, the sharp 1.41 μm band of montmorillonite also does not match the broad 1.4 μm band of the positive opal id material. However, some montmorillonite could be mixed with a majority of amorphous hydrated silica, the sharp montmorillonite signatures being hidden by the broad signatures of the silica.

[35] To sum up, the positive opal id material spectrum is most consistent with that of amorphous to poorly crystalline opaline hydrated silica, locally and/or partially dehydrated, possibly occurring as coatings on basaltic material. This opaline material is intimately or spatially mixed with Fe-oxides/hydroxides/oxihydroxides. We name the corresponding unit "Si" for its hydrated silica content.

4.5. Jarosite-Bearing and 2.21–2.28 Doublet Materials

[36] Figure 4b shows a map of spectral criteria identifying absorptions in the 2.21–2.28 μm range. Apart from Si-OH bearing outcrops discussed above, which show up in cyan,

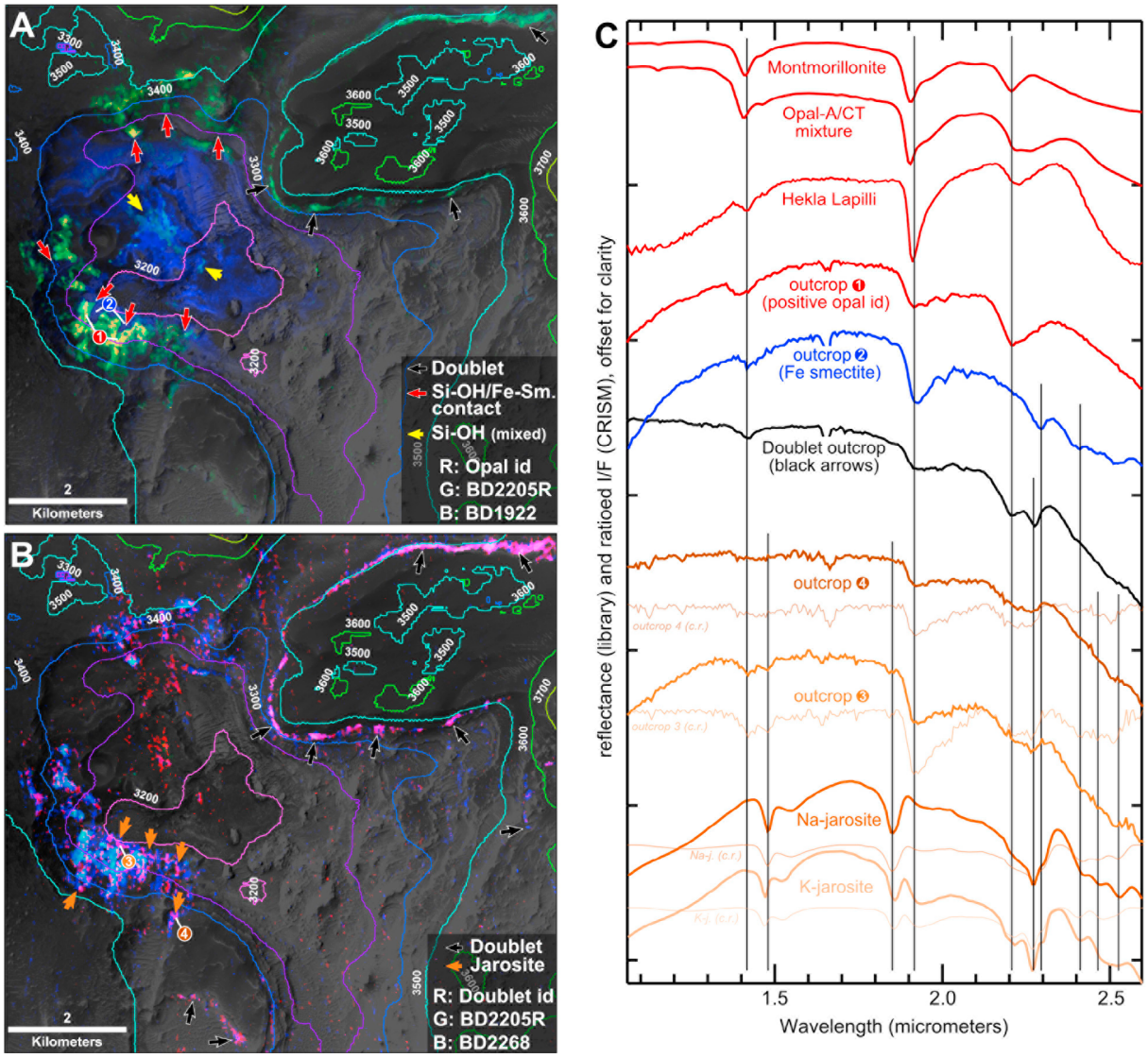

Figure 4. Broad 2.20+ μm band bearing materials. Figures 4a and 4b give RGB composite maps of spectral criteria (source data: see Figure 2). R, G, B channels set to parameters indicated in lower right corner of the maps. Arrows point to outcrops described in the text (also see caption at lower right corner). (a) Map of Si-OH bearing material spectral features. Si-OH bearing material appears in hues from yellow to green for strong to weak signatures. Other hydrated phases are blue. (b) Map of spectral criteria for ~2.2 μm doublet bearing material. Si-OH bearing material appears cyan, ~2.2 μm doublet bearing material appears pink to white (pinpointed by black arrows) and jarosite-rich outcrops appear magenta (pinpointed by orange arrows). (c) Library spectra (top three and bottom two): montmorillonite, opal-A/CT and jarosites are from the USGS spectral library [*Clark et al.*, 2007]; the Hekla lapilli spectrum was acquired in our laboratory. Spectra from outcrops pinpointed in Figures 4a and 4b: outcrop 1 with Si-OH signatures (in red), outcrop 2 with Fe-smectite (in blue), outcrop 3 (in orange), outcrop 4 (in dark orange) and average of doublet outcrops pinpointed by black arrows in Figure 4b (in black). To aid in the identification of weak spectral features, spectra from which the continuum envelope has been removed (labeled c.r., for continuum removed) are superimposed as thin and shaded lines on jarosites and outcrops 3 and 4 spectra.

this map highlights outcrops with positive Doublet index and BD2268, showing up in magenta, pointed out by orange arrows. A spectrum from the lower outcrops, labeled "outcrop 3," is shown in orange in Figure 4c. On this spectrum, we note that the 1.42 μm and 1.9 μm absorptions as well as the 2.3–2.4 μm shape are consistent with a contribution of Fe-smectite, as expected from the juxtaposition of outcrop "3" with the Fe-smectite-bearing material identified previously ("outcrop 2" spectrum in Figure 4c). However, the outcrop "2" and "3" spectra show subtle differences. The spectrum from outcrop "3" has a 1.48 μm shoulder to the 1.4 μm band, a weak 1.85 μm band, a ~2.21 μm

concave upward instead of concave downward shape, a ~2.27 μm instead of 2.29 μm band and a triplet at 2.4–2.5 μm (better viewed on the continuum removed spectra (c.r., shaded)), all consistent with the spectral signatures of Na-jarosite (K-jarosite bands appears slightly shifted compared to this unit's). These spectral properties cannot be accounted for by a material that is Fe-smectite bearing only (which spectrum 2 exemplifies) and point to a Fe-smectite/jarosite subpixel and/or intimate mixture. Besides, the attenuation of absorption bands compared to pure jarosite is similar to that noticed by *Cloutis et al.* [2006] in mixtures with accessory phases such as Fe oxides/hydroxides like hematite and goethite, which might suggest presence of these and/or other phases in this outcrop. Jarosite is a hydroxylated ferric sulfate of formula $(K,Na)Fe_3^{3+}(SO_4)_2(OH)_6$. These outcrops will thus later be discussed with other sulfates. Although these outcrops bear a large component of Fe-smectite, we then differentiate them from the Fe-smectite outcrops of the LSm1 unit on the basis of their jarosite component. We then name the Fe-smectite-plus-jarosite-bearing layered outcrops "LJ" for their jarosite-bearing character.

[37] Figure 4b also shows a unit with positive Doublet Index and BD2205R, pointed by black arrows. Figure 4c shows in black an average spectrum of this unit, featuring a characteristic 2.21–2.28 μm double absorption, or doublet, as discussed by *Weitz et al.* [2011]. A similar doublet feature was also found in Ius Chasma by *Roach et al.* [2010]. The 1.42 μm and 1.9 μm absorptions of this spectrum are consistent with a Fe-smectite component. The 2.21 μm absorption is similar to that of the positive opal id material. The additional ~2.28 μm band, intermediate between the 2.27 μm band of jarosite and the 2.29 μm band of Fe-smectite, could indicate a mixing between hydrated silica, jarosite and Fe-smectite. Alternatively, but not exclusively, as jarosite forms in acidic conditions, this band could sign material resulting from partial acidic dissolution of Fe-smectite. Indeed, experiments conducted on a Al/Fe-smectite (SWa-1) by *Madejová et al.* [2009] showed that the Fe_2-OH 2.29 μm band of the smectite weakened and shifted to ~2.28 μm after 1 h in 6 M HCl. Material featuring this doublet spectrum likely contains hydrated silica with Fe-smectite, possibly partially altered, and jarosite, mixed either spatially or intimately. The layered unit associated with this material is later referred to as "LDb" (Layered Doublet).

4.6. Noctis Labyrinthus Walls and Bedrock Composition

[38] NL cuts through a volcanic plateau of Hesperian age with a surface which is too dusty to provide composition by spectral data. The same goes for the depression walls. Nevertheless, two pits in northern NL display fresh lavas with composition of High Calcium Pyroxene (HCP) rich basalts [*Mangold et al.*, 2010a]. Moreover, Hesperian provinces on Mars have a basaltic composition [e.g., *Poulet et al.*, 2009; *Baratoux et al.*, 2011]. The MER rover Spirit in situ analysis of several rocks also showed that the Hesperian plains covering Gusev crater mostly consist of olivine-bearing basalts [*Arvidson et al.*, 2006b]. Also, among Martian meteorites, the basaltic Shergottites, mostly clinopyroxene (HCP) and plagioclase bearing, are thought to represent the most common lava type on Mars [*McSween and Treiman*, 1999]. We thus assume that, in the studied depression, the primary composition was basaltic too.

5. Morphology and Stratigraphy of Layered Deposits

5.1. Morphology of Units

[39] We describe here the morphological expression of the surfaces of mineralogical units found in the eastern pit within the studied NL depression, going up from the lowest elevation, at ~3180 m, to the highest at ~3500 m. As described in the introduction of section 4, we note that among mass wasting and landslide deposits overlaying the floor of the depression, some overlay part of the layers visible in the pit. Figure 5 shows the location of subsequent figures (Figures 6, 7, 9, 10, 11, and 12) on a visible and on a simplified spectral map of the pit. For clarity, when naming units, we use the terminology "*mineral* unit" instead of "*mineral bearing* unit," where "*mineral*" is the name of the mineral characteristic of a unit, as defined in section 4. This terminology does not preclude the presence of other minerals within each unit.

5.1.1. Sulfate Units

[40] Sulfate bearing outcrops are shown in Figure 6. We can distinguish two types of sulfate outcrops: one type from what we then call the "main sulfate unit," and another type from sulfate material scattered within other units. Both are bright relative to surrounding terrains. The main sulfate unit has a large surface exposed, showing ENE-WSW trending dune-like structures tentatively interpreted as eolian bed forms (Figure 6a). Layered deposits bearing polyhydrated (LSH), monohydrated or hydroxylated (LSD) sulfates all show surfaces covered with rock slabs ranging in width from less than 1 m to 6 m (e.g., Figure 6b). Some blocks cast shadows ~1 m long, which translate to ~1 m height with the sun 47° above the horizon. Along with characteristic spectra, this morphology allows identification of numerous, apparently isolated, sulfate-rich outcrops (Figure 6c) within the overlying smectite unit LSm1. At least one sulfate layer stands out within the overlying deposits (Figure 6d) and was chosen to mark the base of "LSB" unit (for Layered unit with Sulfate Basal layer), sealing unit LSm2. LSB unit is characterized by thin layering and bland spectra, aside from its Fe(OH) sulfate basal layer.

[41] Jarosite signatures are detected in two types of outcrops. The first one has the strongest jarosite signature (though mixed with Fe-smectite). It is outlined in Figure 6e and corresponds to outcrop 3 in Figure 4. It forms an area of barely noticeable heterogeneity in brightness and degree of fracturation within the lower Fe-smectite unit (LSm1). A second type of jarosite outcrop, shown on Figure 6f, has a weaker jarosite spectral signature (see outcrop 4 in Figure 4). It appears to be the flat surface of a distinct layer with a blockfield aspect not unlike that of other sulfate outcrops, supporting the identification of jarosite despite very weak spectral features.

5.1.2. Halloysite and Si-OH Units

[42] The halloysite unit (H) is bright and massive, and partly covered with polygonally dissected dark and smooth material (Figure 7a). This morphological expression is always

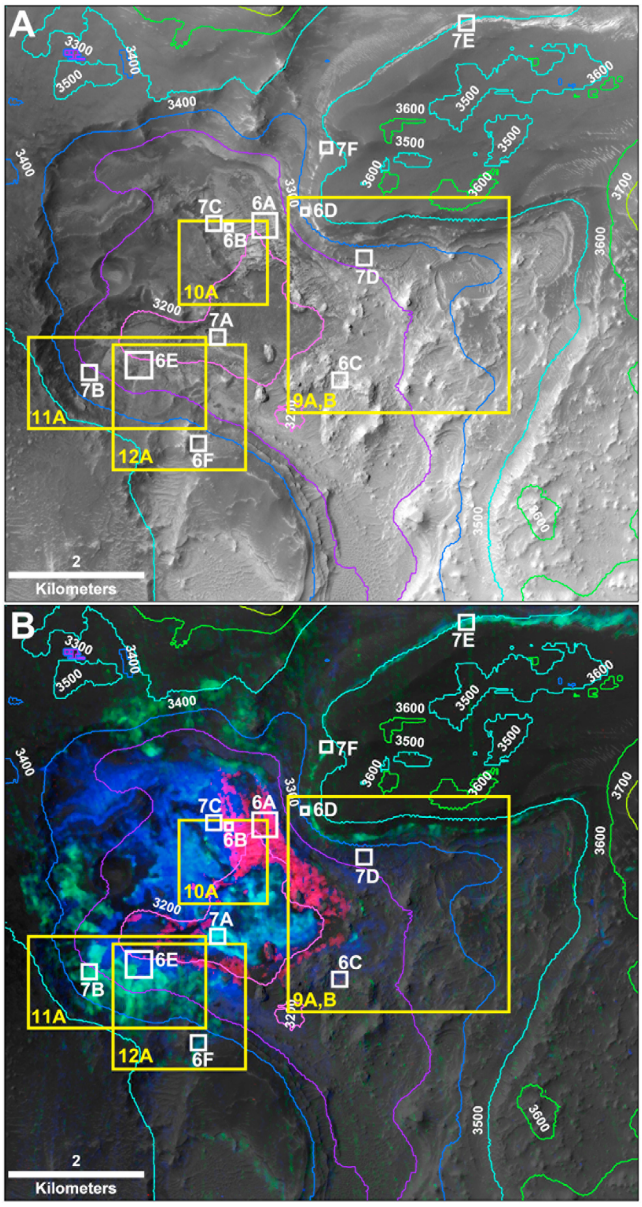

Figure 5. Localization of outcrops shown in subsequent figures (Figures 6, 7, 9, 10, 11, and 12) showing the morphology of the different units (white boxes and labels) and stratigraphic relationships (yellow boxes and labels). Background is a CTX image with (a) HRSC contours and (b) overlay of CRISM RGB composite of spectral parameters (R: Sulfate Index, G: BD2205, B: BD1922) where it is possible to identify main phases such as Si-OH bearing material in green, halloysite in cyan, sulfates in pinkish hues and other hydrated minerals (mainly Fe-smectite) in blue.

correlated with halloysite-like spectra where the surface exposed spans enough CRISM pixels for the spectral data to be conclusive. We thus used this morphology to identify the extent of the halloysite unit also from smaller outcrops.

[43] Si-OH bearing outcrops appear dark, heterogeneous, and show no layering. An area with strong Si-OH signature is shown on Figure 7b. Some outcrops bear bright to dark meter-scale blocks, scattered within a matrix of variable brightness.

5.1.3. Fe-Smectite Units

[44] Outcrops from the lower Fe-smectite (LSm1) unit (Figure 7c) are darker than sulfate or halloysite outcrops. They show that this unit is finely layered, and cut by fractures or veins with spacing from 1 to 10 m. Contrary to sulfate outcrops, lower smectite outcrops rarely shed individual blocks and remain cohesive, despite appearing fractured. The upper smectite unit (LSm2) outcrops (Figure 7d), with lower spectral signatures, are darker, with a smooth and homogeneous morphology suggesting a cover of sand-sized material.

5.1.4. Doublet Unit

[45] An outcrop of the doublet unit is shown on Figure 7e. All of them are bright and show sinuous shapes consistent with soft deformation of layers. There is an angular unconformity (Figure 7f) between the pile of layered deposits filling the eastern part of the pit and the doublet unit at its top. The irregular shape of the depression rims and walls, as well as the mantle of debris on the walls, are consistent with mass wasting from the depression walls. Given the mixture-like spectral signature of the doublet unit, the deformation and unconformity observed are consistent with this layer being a result of the energetic sliding of a landslide on a former ground surface. The friction at the landslide base would have promoted the mixture of several layers (bearing Fe-smectite, Fe-sulfates like Fe(OH) sulfates and jarosite, and Si-OH bearing material).

5.2. Stratigraphy

5.2.1. Geologic Map and First Order Units

[46] From integrated geological analysis of textural, morphological and spectral observations, we have built a geologic map of the pit, presented on Figure 8 with a reference stratigraphic section. Figure 9 shows imaging of a selected area of the pit with an overlay of CRISM spectral parameters (Figure 9a) and of the geologic map (Figure 9b) with respective perspective renderings in Figures 9c and 9d. These views show the subhorizontal succession of the most prominent units, from bottom to top: the halloysite unit, massive (H); then the following layered units: the sulfate unit from ~3200 m to ~3240 m (LSD/LSH), the lower smectite unit up to ~3300 m (LSm1), the upper smectite unit up to ~3400 m (LSm2), a bland layered unit of various thickness (LSB, defined by a sulfate layer at its base at ~3400 m), and the deformed doublet unit (LDb). These units are capped by a dark, bland, massive and boulder-shedding unit (unit C; see Figure 8). Where LDb is present, i.e., in two locations, to the east and south of the pit, landslide tongues have locally covered the pre-existing layered deposits with erosion-resistant material. This armoring shielded the layered deposits from the subsequent erosion that formed the current pit. The Si-OH unit (Si) is visible on the walls of the pit where they are exposed, at elevations from ~3250 m to 3500 m (Figure 8), and does not appear layered. Notably, some Fe-sulfate (Fe(OH) sulfates and jarosite) layers occur within smectite units at various elevations (LSD/LJ).

5.2.2. First Order Stratigraphy of Halloysite, Sulfate and Smectite Units

[47] The halloysite (H) unit is mostly observed at the center of the pit, at the lowest elevations. The largest exposure covers the bottom of the pit, from ~3200 m downward. Outcrops with the same spectral and morphological

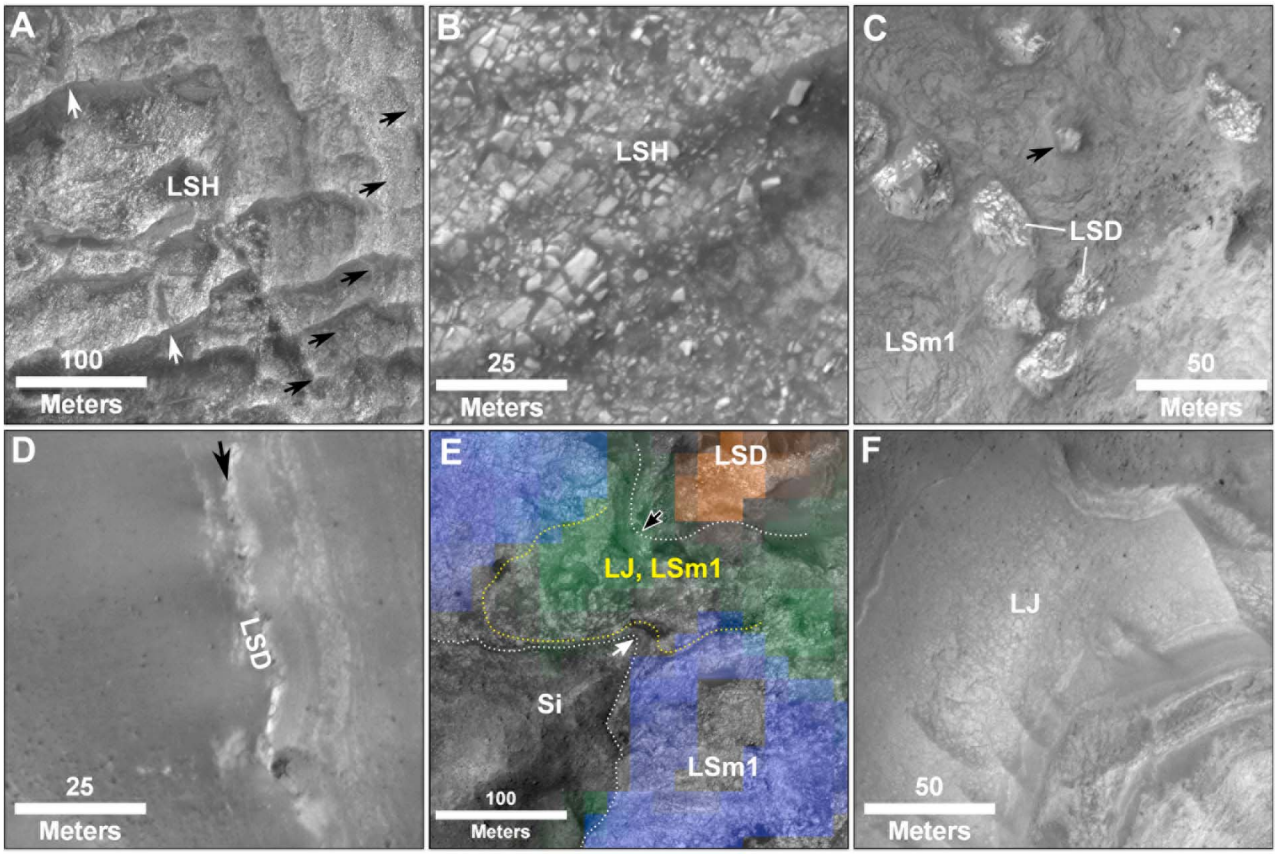

Figure 6. Fe-sulfate bearing outcrops from HiRISE images. Acronyms refer to unit names explained in the text. (a) Subset of the largest exposure of layered polyhydrated Fe-sulfate-rich material. Black arrows point to ~N-S trending successive outcropping layers. White arrows point to ~ENE-WSW trending structures tentatively interpreted as fossil eolian dunes. (b) Close-up view of sulfate bearing material showing typical blockfield aspect with scattered smooth blocks or slabs <1 m to 6 m large. (c) Area of outcropping bright patches (15–50 m across, with 1–6 m wide slabs) of sulfate bearing material surrounded by a smooth matrix of darker Fe-smectite bearing material. Black arrow shows a small mound of smectite material topped and armored by sulfates. (d) Distinct layer (black arrow) of Fe(OH) sulfate material eroding away from the stack of deposits on the eastern wall of the pit; defines the base of LSB unit. (e) Jarosite outcrops within the lower smectite unit at the bottom of the SW wall of the pit. HiRISE image with overlay of CRISM spectral parameters color composite (orange for Fe-sulfates, except jarosite, green for jarosite, blue for Fe-smectite). Jarosite signatures lie within yellow dotted line. Black arrow points are contact of smectite unit over sulfate unit. White arrow points are contact of smectite unit over Si-OH unit. (f) Jarosite bearing outcrop on the S wall of the pit at ~3400–3450 m. Note the blockfield aspect (1–3 m wide slabs) similar to other Fe-sulfate bearing outcrops.

characteristics occur at higher elevations (~3200 to ~3350 m, pointed by white arrows in Figure 3a), in contact with sulfate or smectite units. The halloysite bearing material could be an early deposit, emplaced before all other units, and intimately draping the bedrock. However, its presence at various elevations and its apparent higher strength favor the hypothesis that halloysite is present in the bulk of the bedrock or that it corresponds to a duricrust capping the bedrock.

[48] The main sulfate (LSH/LSD) unit is continuous from ~3200 m to ~3240 m. On the halloysite bearing floor of the pit (yellow circles in Figure 2b), two remnant buttes of sulfates are evidence that the sulfate unit was once continuous and has been eroded away. At the bottom of the pit, the contact of the layered LSH/LSD unit over the H unit is subhorizontal (Figure 8a). The relative stratigraphy of halloysite, sulfate and smectite units is shown in Figure 10. The sulfate unit overlies the halloysite unit; both, when their contact is exposed, are overlain by the onlapping smectite unit. Smectite outcrops are never found at elevations lower than the top of the sulfate unit, at ~3240 m, consistent with the deposit of LSH/LSD followed by the Deposit of LSm1/2.

5.2.3. Draping of Layered Deposits Over the Bedrock

[49] In Figure 11, in addition to the horizontal contact of smectite over sulfates at the bottom of the pit, Fe-smectite material pertaining to layered units can be seen preserved within two re-entrants in the SW wall of the pit, separated by a Si-OH bearing spur. Layered material can be tentatively traced up the re-entrants to more than 3400 m in some locations, close to the highest elevation of layered material all over the pit. Figure 12 also shows a location where

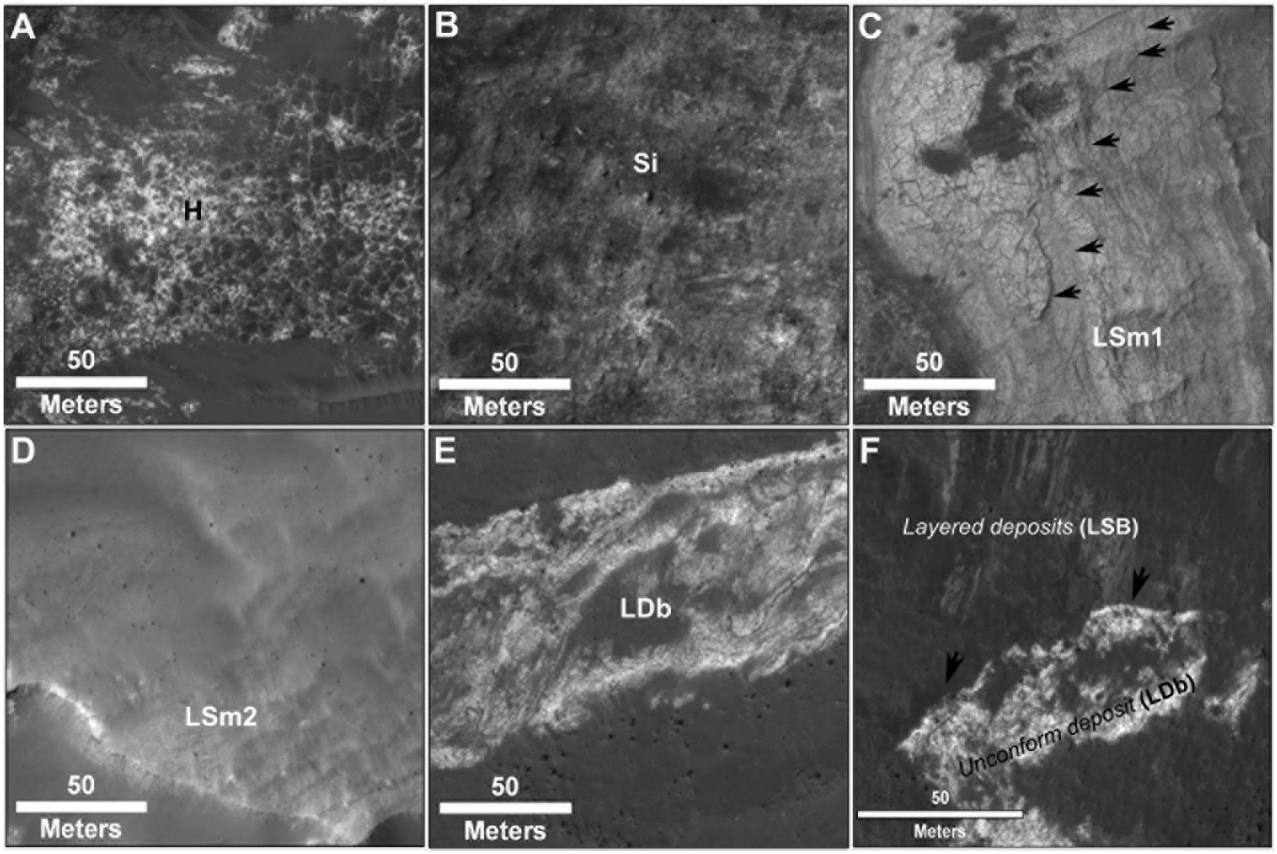

Figure 7. Outcrops of non-sulfate-bearing units. (a) Halloysite unit (H): bright and massive where exposed (center-left), it is partly covered (on the right) with a dark and smooth unit forming polygons ~2 to ~10 m large; the halloysite bearing unit is exposed between polygons. (b) Typical area of strong Si-OH signature (Si unit), on the SW wall of the pit, heterogeneous in brightness and texture. (c) Lower Fe-smectite unit (LSm1) showing a smooth surface with widely spaced fractures and thin layering. Arrows point to ~NNW-SSE lineaments formed by individual outcropping layers. (d) Upper Fe-smectite unit (LSm2). (e) Doublet unit (LDb) outcrop (bright) emerging at the base of a probable landslide deposit (bottom of picture, with blocks). Curved structures are interpreted as soft deformation (folds) within the doublet unit. (f) Unconformity (black arrows) between layered deposits unit LSB and overlying doublet unit LDb.

layered deposits clearly embay a Si-OH bearing bedrock spur (Figure 12a for context, Figure 12b for close-up and Figures 12c to 12f for complete interpretation). Similar observations can be made all around the pit, on its walls: unlike what is observed at the bottom and center, contacts of layered smectite units (LSm1/2) over H and Si-OH (Si) units all dip toward the center of the pit, at various angles (2 to 14 degrees, as reported in Figure 8a). This is consistent with a draping and cementation of the layered units (first LSH/LSD, then LSm1/2 and LSB) all over a "proto" pit, up to ~3500 m, over a non-layered bedrock now including the H and Si units. Subsequent erosion has removed layered material mostly to the west of the "proto" pit, forming the current pit. This erosion was able to remove layered units likely because of their weak strength against eolian erosion compared to bedrock units. Conversely, to the east and south, the deposit of landslide material has armored the layers, preventing their erosion. The current pit is therefore smaller in size than the proto pit which likely extended laterally a few kilometers more to the south and east of the chasma.

5.2.4. Genetic Relation Between Si-OH Material and Other Units

[50] Si-OH bearing bedrock is found on the walls and at the periphery of the pit. Though found at various elevations, it is locally always above halloysite-bearing bedrock. To the north, Si-OH bearing material can be identified up to slightly above 3500 m. This elevation is also the highest reached by layered deposits (as can be observed to the east of the depression, outside of the pit). The lowest outcrops of Si-OH bearing bedrock are located on the southwestern wall of the pit, where stratigraphic relationships with layered units are most visible.

[51] The heterogeneous morphology of the Si-OH unit at HiRISE scale (Figure 7b), despite a rather homogeneous signature at CRISM scale, may indicate that the Si-OH bearing material is surficial, perhaps in the form of small grains, silcretes, rinds or coatings, blanketing the underlying basement. Most prominently, as showed in the previous

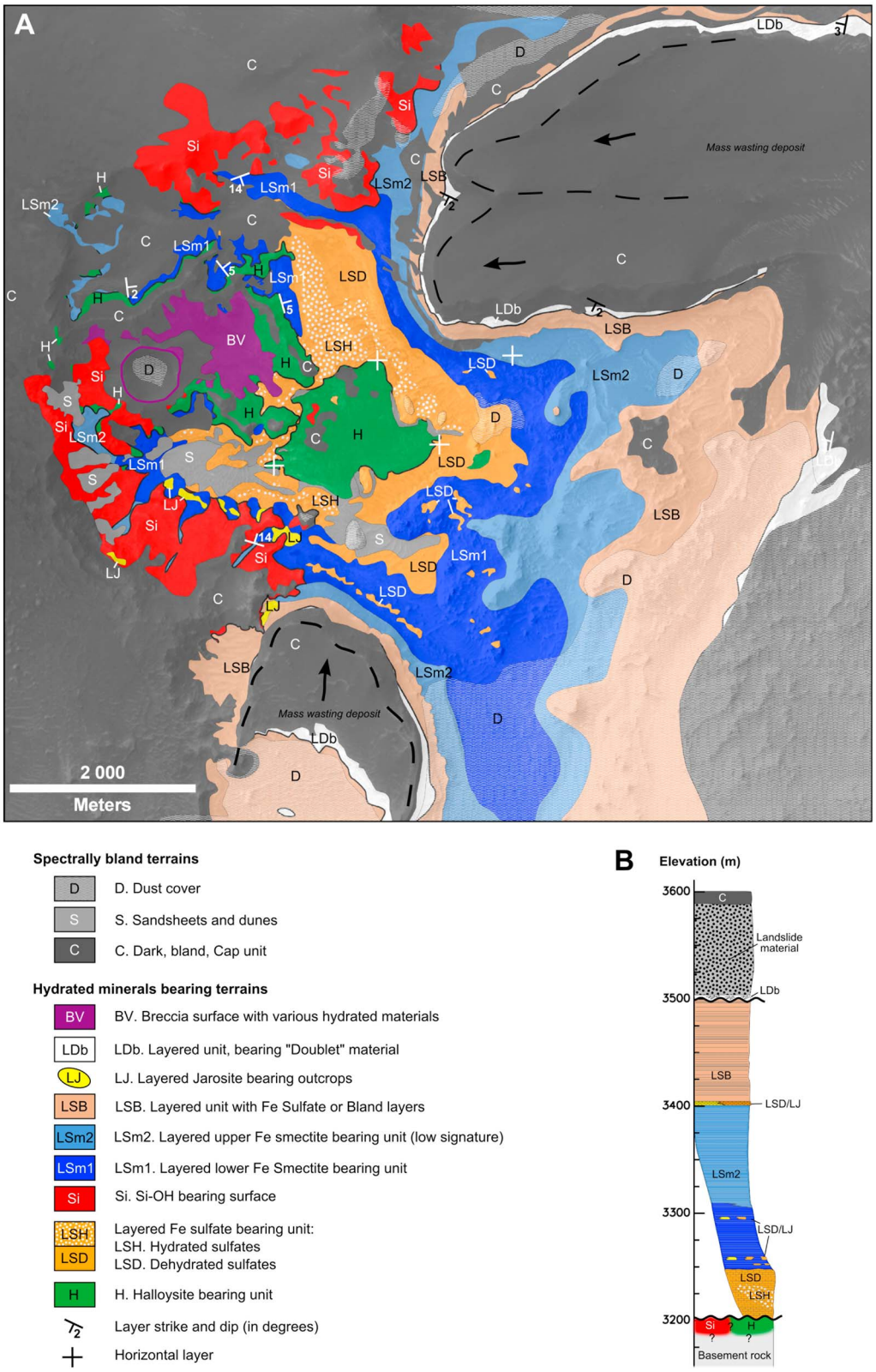

Figure 8. (a) Geologic map of the pit overlain on CTX image, with caption for reference to acronyms on the map. Layered units, exclusively, have been labeled "L…" for clarity. Names of units are based on their spectral characteristics. Thicker contours have been used to highlight unconformity stratigraphic contacts where visible. Conventional symbols indicate layer strikes and dips (in degrees) where measured. (b) Stratigraphic section of units identified in the map. Unconformity contacts are marked by thick wavy curves.

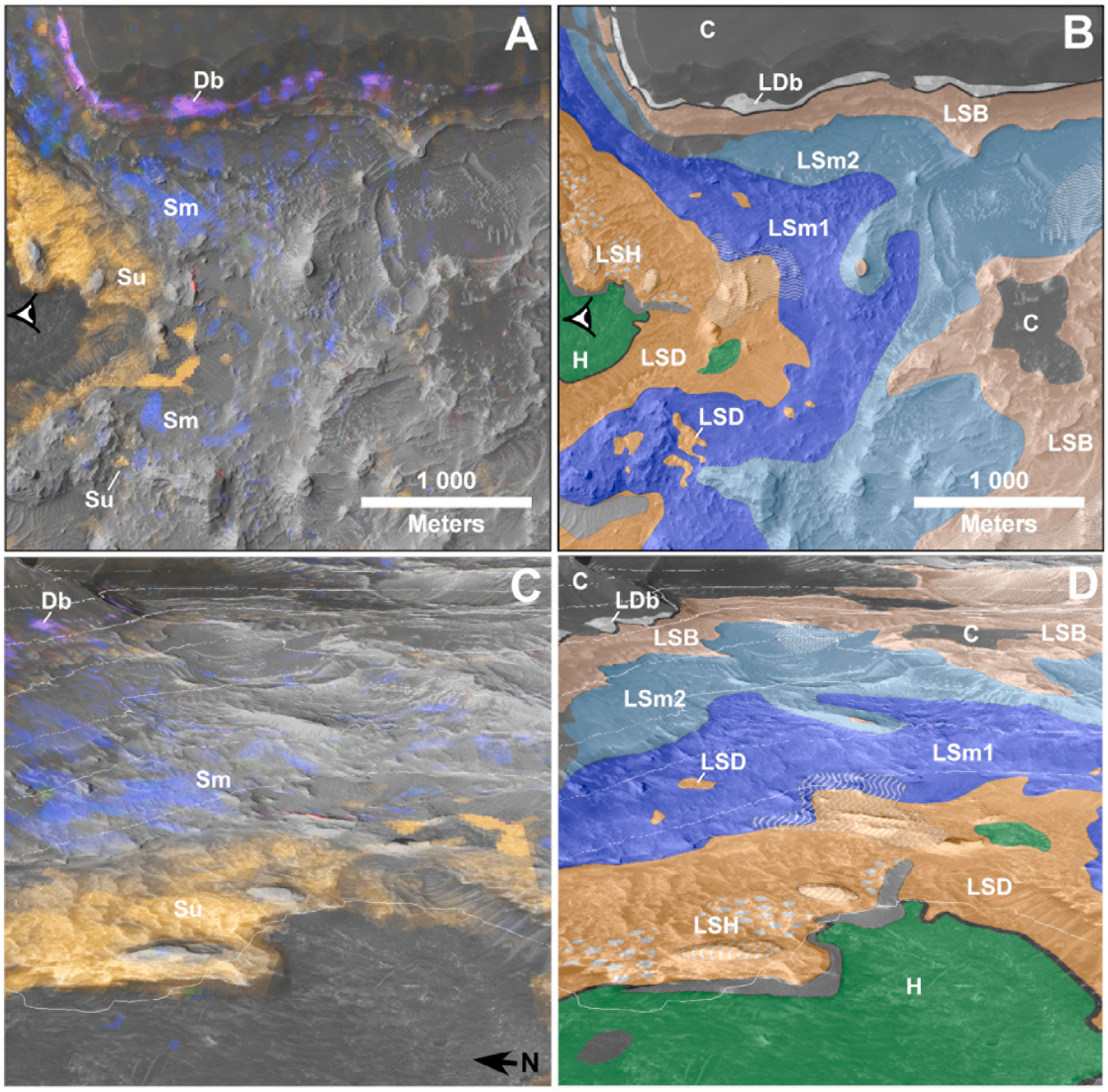

Figure 9. Stratigraphic relationships between Fe-sulfate, Fe-smectite and doublet units. (a) Context morphology from HiRISE image with overlay of CRISM spectral parameters (color composite: Fe-sulfates (except jarosite) are orange, doublet signatures are magenta and Fe-smectite is blue). (b) Same extent as Figure 9a with geologic map overlay (cf. Figure 8 for caption). Eye symbol in Figures 9a and 9b indicates vantage point for Figures 9c and 9d perspective views. (c) Same as Figure 9a in perspective view from the west. (d) Same as Figure 9b in perspective view from the west. Figures 9c and 9d vertical exaggeration: $\times 2$.

section, the layered Fe-smectite units have been deposited over the Si (and H) bedrock all over a "proto" pit before erosion removed most or only a little of the deposits, depending on the location.

[52] Together, these observations lead to the following hypotheses: the Si-OH bearing material is either (1) a leftover of the eroded smectite units, perhaps in the form of grains that are more resistant to erosion than smectite minerals, or (2) a rind or coating on the bedrock, formed either before or after emplacement of the layered deposits. The former case is difficult to reconcile with observations of layered smectite material directly onlapping halloysite bearing bedrock without exposure of Si-OH material (cf. supra).

[53] We thus favor the hypothesis that Si-OH material is a coating or duricrust on the bedrock and not leftover material from the layered deposits. Still, interaction between bedrock and layered materials could have played a role in the formation of the Si-OH bearing material under local conditions.

5.2.5. Interbedded Sulfate Layers

[54] In this section, we examine the case of sulfate layers occurring within smectite and bland units. From morphology, several sulfate patches, 10 m to 50 m wide, can be identified at ~3260 m and ~3300 m (Figure 6c). Spectra confirm the identification with the 2.23 μm band of Fe(OH) sulfates (see alternating orange, for sulfates, and blue, for Fe-smectite in Figure 12). It is not clear from HiRISE images if some of these outcrops actually occur because of erosional windows through overlying smectite layers. However, other patches clearly are sitting on top of and armor underlying

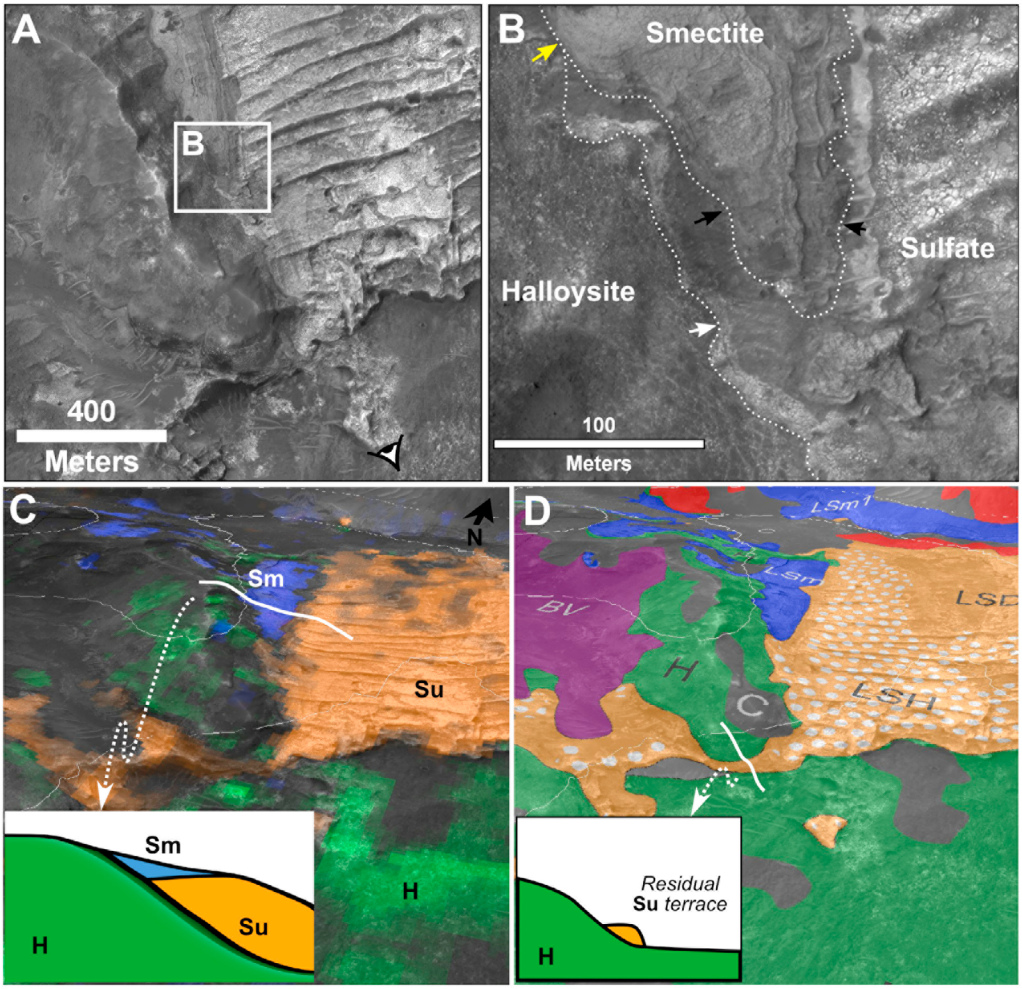

Figure 10. Stratigraphic relationships between halloysite, sulfate and smectite units. (a) Context morphology. Eye symbol indicates vantage point for C and D perspective views. (b) Close-up on triple contact: Sulfate unit overlies halloysite unit (white arrow), smectite unit overlies sulfate unit (black arrows) and halloysite unit (yellow arrow). (c) Perspective view from the SSE with spectral map draping (color composite: sulfates (Su) are orange, halloysite (H) is green, Fe-smectite (Sm) is blue). 2× vertical exaggeration. (d) Same perspective view with geologic map draping. White lines in Figures 10c and 10d mark ground tracks of schematic interpretative cross-sections in respective lower left corners.

smectite layers (Figure 6c, arrow). Smectite unit layers are preferentially eroded around sulfate patches, forming mounds of smectite-bearing material topped by sulfates. These sulfate-bearing patches could be the remnants of a continuous sulfate layer which has been mostly eroded away. In this case however, we would expect to find at some places a preserved continuous outcrop; but none has been found. Alternatively, these sulfate patches could be evidence of multiple local occurrences of sulfate deposition: in this case continuous sulfate layers would never have existed at these elevations, suggesting either lateral variations in the composition of deposits and/or in subsequent alteration.

[55] Another Fe(OH) sulfates bearing layer is visible at ~3400 m within the pile of deposits on the eastern wall of the pit (Figure 6d). We identify that layer with the second outcrop of jarosite described in section 5.1.1 (Figure 6f). It is found in the pile of deposits forming the southern wall of the pit, at a similar elevation. It seems plausible that jarosite, a hydroxylated Fe-sulfate, and other Fe(OH) sulfates may coexist in a single layer, with horizontal compositional variations. Both outcrops may therefore be remnants of a unique layer formerly spanning the whole pit. Different ages of exposure or outcropping conditions may also reveal one signature or the other. Alternatively, two or more layers of different composition are superposed near ~3400 m and outcrop more or less on one side of the pit or the other.

[56] The first jarosite rich outcrop described in section 5.1.1 is at ~3250 m of elevation (Figure 6e). With both Fe-smectite and jarosite spectral features, it is consistent with the occurrence of a thin jarosite rich layer within the lower smectite unit, and uneven erosion revealing both materials at almost the same elevation. The ~3260 m Fe(OH) sulfates and ~3250 m jarosite patches may be evidence of a unique sulfate rich layer, or of multiple sulfate spots within the smectite unit.

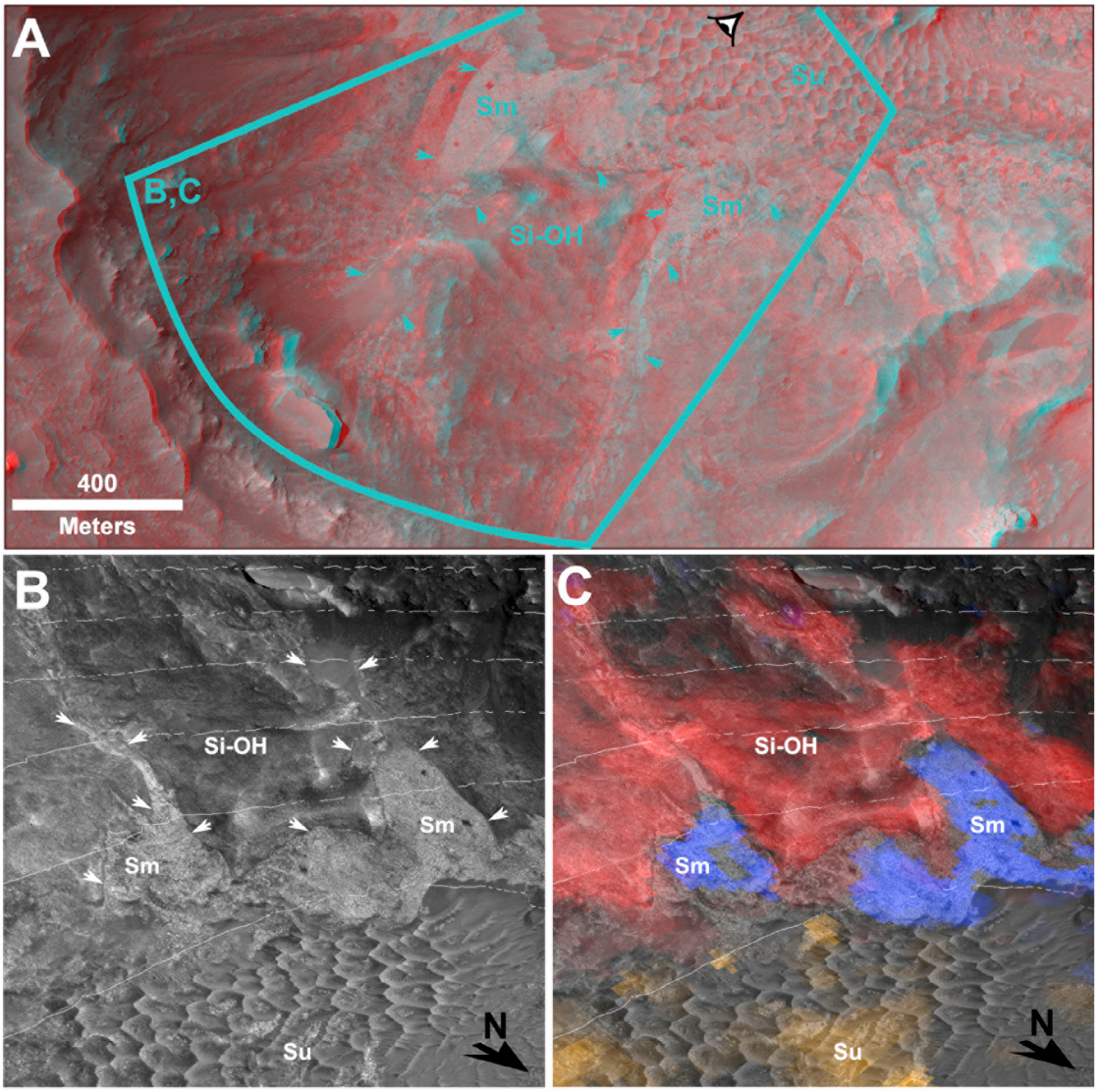

Figure 11. Stratigraphic relationships between layered Fe-smectite unit and Si-OH bearing bedrock. (a) Subset of HiRISE anaglyph ESP_019377_1695_ESP_016898_1695_RED, to view with red/blue glasses, covering the southwestern wall of the pit. Contact between Fe-smectite (Sm) and Si-OH bearing material is pointed out by arrows. Su for sulfates. Eye symbol for vantage point for Figures 11b and 11c perspective views. (b) Perspective view from the NE showing the same contact as in Figure 11a (coverage shown by curved box in Figure 11a). 2× vertical exaggeration. Arrows point to the contact between layered Fe-smectite (Sm) and massive Si-OH bearing materials in two re-entrants in the pit wall. (c) Same perspective as Figure 11b with overlay of CRISM spectral parameters for Si-OH (red), Fe-sulfates (orange) and Fe-smectite (blue).

5.3. Constraints on Ages

[57] The sealing of all layered deposits by landslides gives a lower age constraint on the time of deposition within the pit. We counted craters on a ~4 km^2 area over the landslide at the NE of the pit. A crater production function (PF) fit [*Michael and Neukum*, 2010] on 36 craters larger than 30 m yields an age between ~80 and ~140 Ma (Figure 13a). This low crater retention age is consistent with recent erosion within the depression and does not constrain much the time of deposition. An upper age limit may be given by crater retention on the depression floor surface, where infilling has not taken place. We identified an homogeneous, highly cratered, ~10 km^2 area to the west of the depression. The age determined by PF fit is between ~3.1 and 3.6 Ga (Figure 13b), i.e., close to the admitted age of formation of NL depressions, i.e., Late Hesperian. Therefore, crater counting dating, due to low retention of craters because of erosion, cannot constrain the ages of the pit deposits better than being posterior to NL depressions formation at the end of the Hesperian, and older than ~100 Ma. It nevertheless shows that deposition and alteration occurred after the period usually admitted to be wet and warm.

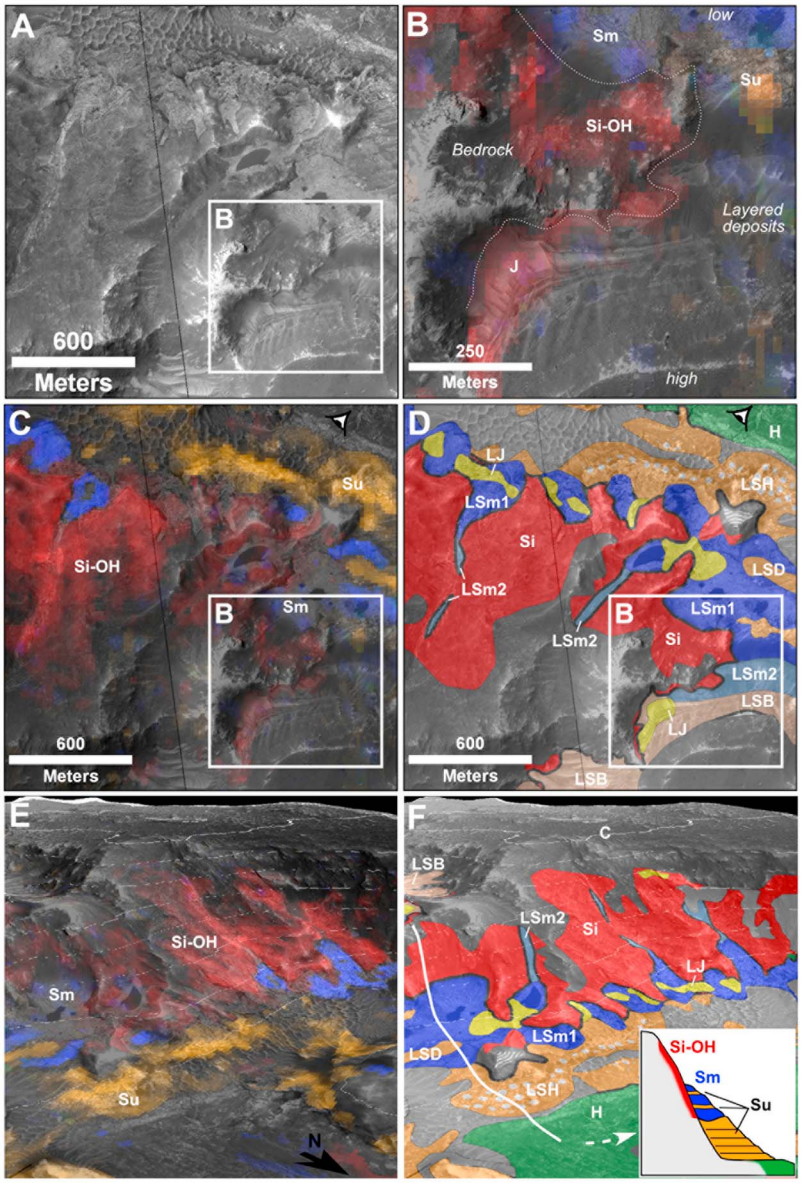

Figure 12. Stratigraphic relationships between Si-OH, sulfates and smectite units. Su: Fe-sulfates; Sm: Fe-smectite; J: jarosite. (a) Context morphology from HiRISE images. (b) Close-up with CRISM spectral parameters overlay (color composite: red for Si-OH, orange for Fe-sulfates (except jarosite) and blue for Fe-smectite) showing pit wall (with Si-OH signatures) partly buried under layered deposits. White dotted line highlights the contact. (c) Same extent as Figure 12a with same CRISM overlay as Figure 12b. (d) Same extent as Figure 12a with geologic map overlay (cf. Figure 8 for caption). Eye symbol indicates vantage point for Figures 12e and 12f perspective views. (e) Same as Figure 12c in perspective view from the NE. Note alternating orange and blue (i.e., sulfate and smectite) layers at lower left. 2× vertical exaggeration. (f) Same as Figure 12d in same perspective as Figure 12e. White line is ground track of schematic interpretative cross-section in lower right corner.

5.4. Summary and Implications

[58] We can synthesize all observations from spectra, morphology and stratigraphy on a cross-section of the pit, shown on Figure 14. This cross-section can be approached considering three classes of units with hydrated minerals:

[59] (1) units bore by the bedrock, either in bulk or as coatings or duricrusts: H (halloysite or other kaolin-group minerals) and Si (Si-OH material) units;

[60] (2) units of layered deposits spanning the whole pit, from bottom to top: LSH/LSD (hydrated and dehydrated Fe-sulfates) main unit, LSm1 (Fe-smectite) and LSm2 units, LSB (layers with a distinctive basal Fe-sulfate layer) unit;

[61] (3) the summital LDb (doublet material, interpreted as jarosite, Si-OH, Fe-smectite mixture) unit at the base of landslide materials.

[62] In addition, some layers show (4) lateral variations in composition such as patchy LSD (dehydrated Fe and

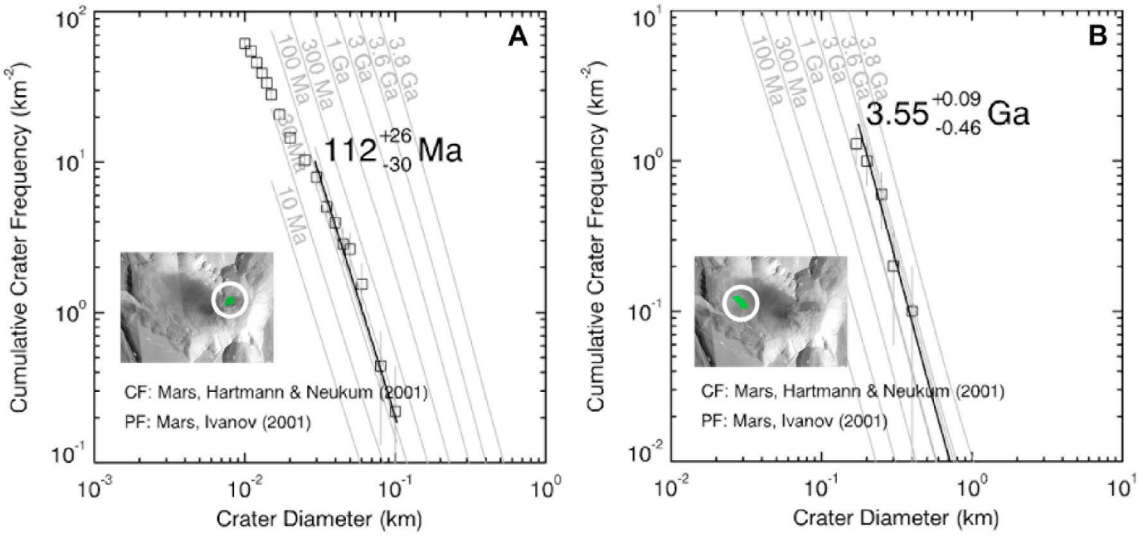

Figure 13. Crater counts for the studied depression. Boxes show cumulative crater frequency with error bars. Black curve is best fit to production function with corresponding age. The green area circled in white shows the surface examined in each case. (a) Crater population for the uppermost unit on top of a mass-wasting landform (total of 36 craters >30 m over 4.55 km^2). (b) Crater population for the most preserved area of the uncovered depression floor (total of 13 craters >180 m over 10 km^2).

Fe(OH) sulfates) and LJ (jarosite) units at various elevations within layered deposits.

[63] From a mineralogical point of view, these units show, associated in close proximity: Al and Fe rich clays, hydrated silica, Fe-sulfates and Fe-oxides; all of which are typically formed in various conditions on Earth, and are not expected to be found together.

[64] Transport from pre-existing alteration zones could explain this diversity. However, hypothetical transport paths and source regions for the layered materials identified in this study have not been found. If the aqueous alteration minerals currently visible within the pit were formed elsewhere and transported, there is no evidence to support it (e.g., no river channel). The lack of transport path for layered deposits therefore implies an in situ formation of hydrated minerals.

[65] Clay formation, as shown by numerous studies of terrestrial weathering environments [e.g., *Garrels and Christ*, 1965; *Eberl et al.*, 1984, and references therein], is strongly dependent on the composition and pH of the alteration solution, related to the amount of rainfall (water input) and drainage (removal of leachates from the system): smectites form in concentrated, neutral to alkaline solutions where most cations are retained, kaolinite/halloysite in more dilute, mildly acidic solutions, and gibbsite (not observed) precipitates in high leaching settings with low Si activity. Halloysite and kaolinite may form from ultramafic to granitic rocks, and result from weathering or hydrothermal alteration. Still, they occur consistently in high moisture to water-saturated settings [see *Joussein et al.*, 2005, and references therein], i.e., at high water-to-rock ratio, and require a minimum silica activity to form. Typical pHs of halloysite formation are in the 3 to 6 range [*Ece et al.*, 2008]. In contrast, Fe-sulfates precipitate from acid sulfate solutions at low pH, from pH < 4 (for jarosite, typically stable at pH ∼ 1–4 [*Brown*, 1971; *Burns*, 1987; *King and McSween*, 2005]) to very acidic solutions at pH ∼ 0 (for ferricopiapite or rhomboclase [*Majzlan et al.*, 2006; *Ling and Wang*, 2010]).

[66] For reference to geochemical constraints, minerals observed in this study have been placed in a redox potential (Eh) versus pH diagram (Figure 15) adapted from modeled data for K-Fe-S-H solutions [*King and McSween*, 2005], modeling of acid weathering of basalt [*Zolotov and Mironenko*, 2007], and experimental data for clays and silica [*Harder*, 1976].

[67] The minerals observed in this study do suggest a role played by: (1) neutral to alkaline waters at low water-to-rock ratio (Fe-smectite), (2) mildly acidic waters at high water-to-rock ratio (halloysite) and (3) saturated acid sulfate solutions (Fe-sulfates). Thus, any scenario aiming to explain the formation and alteration of the units observed in the studied depression has to take into account this diversity of alteration solutions. However, we will show that distinct environments are not required to explain the large diversity of aqueous alteration minerals that we identified.

6. Discussion

[68] In this section we discuss the sequence of events and the processes of emplacement and modification of the units found in the pit.

6.1. Geological Context

6.1.1. Origin of Layered Sediments

[69] We examined in detail the eastern pit of one depression of NL where two comparable pits show exposed layers. We identified, for the eastern pit alone, a ∼300 m thick stack of layered material, exposed by erosion and thus partially removed, but originally spanning ∼100 km^2. This represents a volume of ∼30 km^3 of layered material. Impact ejecta are possible contributors, but would not account for

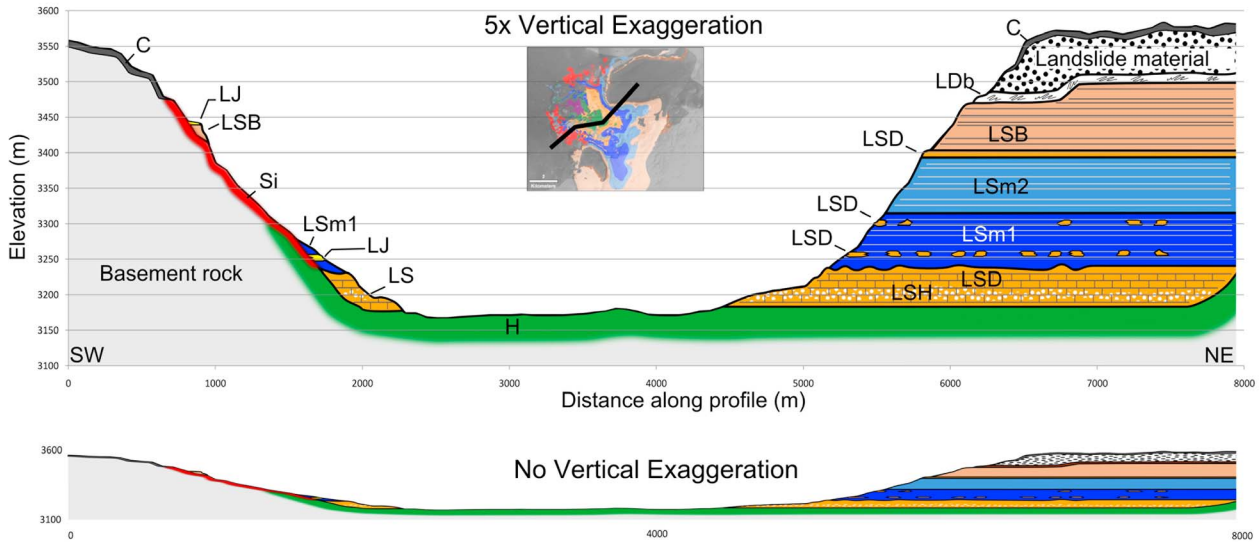

Figure 14. Cross-section across the pit from SW to NE with 5× vertical exaggeration for clarity. The same cross-section is duplicated below with vertical exaggeration removed to give a fair representation of the planar nature of the deposits.

the overall thickness and diversity of material. While the current limited extent of the deposits in the lowest pits could argue for selective transport by aqueous pathways and deposition of detrital sediments in an open lake, it is excluded from the lack of any fluvial landforms or lake shoreline. We thus favor two processes: (1) dry processes such as air fall deposits (volcaniclastic or eolian), applying for the main thickness of layered material deposited, then followed by in situ alteration and (2) precipitation of hydrated phases out of solution, that could account for local enrichment in sulfates, for example.

[70] The depression studied in this paper is located within a 1300 km radius of Arsia, Pavonis and Ascraeus Montes. Modeling of Plinian eruptions from these volcanoes, incorporated in a global circulation model of the Martian atmosphere, shows that volcanic ashes from these volcanoes, notably Arsia Mons can reach Noctis Labyrinthus [*Kerber et al.*, 2008], providing a source for the air fall material. Comparison with Earth volcanic ash beds supports the hypothesis of the volcanic air fall origin of the layered deposits studied. Tharsis calderas, tens to a hundred km in diameter, are comparable to that of Earth's Yellowstone hot spot. At comparable distance (∼1000 km), the latter deposited ash tuffs 0.1–4 m(s) thick during each of its major eruptions in the last 16 My (1–6 per My), with a total ash discharge of ∼0.5–2 × 10^3 km^3/My [*Perkins and Nash*, 2002], and a few times more total erupted or extruded magma. For rates of magmatic activity of Martian volcanoes, several authors have used the rate of Earth's Hawaii-Emperor chain rate over the last 65 My of ∼10^4 km^3/My [*Robinson et al.*, 1993; *Plescia*, 2004], similar to the Yellowstone rate [*Christiansen*, 2001]. For a first order comparison, we assume those rates of magmatic activity around Noctis Labyrinthus. Assuming the higher end of Yellowstone ash tuffs deposition rate (∼24 m/My) we find that 300 m of volcanic ashes may be deposited in ∼12.5 My. Rapid eolian remobilization of air fallen material and

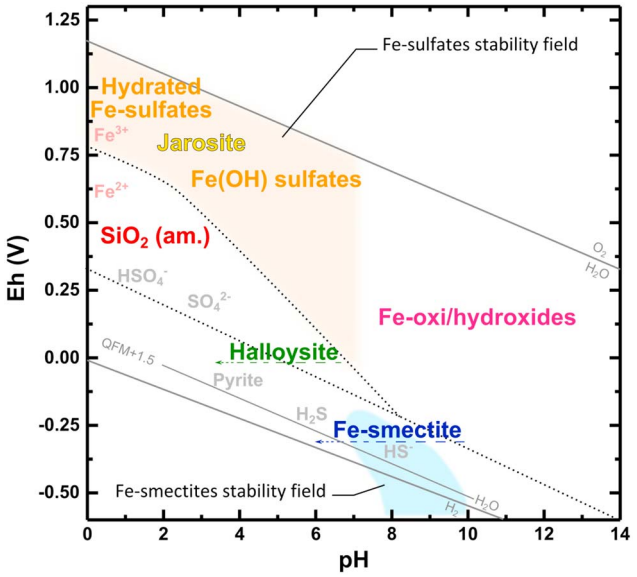

Figure 15. Eh versus pH diagram, adapted from *King and McSween* [2005] for acid sulfate solutions and minerals relevant for Mars. Fe and SO_4^{2-} activities in the 10^{-4}–10^{-2} range. Silica and clays stability fields adapted from *Harder* [1976] and *Zolotov and Mironenko* [2007]. Quartz-Fayalite-Magnetite (QFM) +1.5 line indicates Eh upper limit for Martian rocks [*Dyar et al.*, 2005]. The Martian atmosphere plots are at the H_2O/O_2 limit. For reference, we indicate dominant sulfur/sulfate and Fe species in shaded gray and pink, respectively. Observed minerals have been placed with their name in colors corresponding to the geological map. Boundaries between minerals would shift by a few 0.1 V and/or a few pH units with various solute activities. All observed minerals fit in the diagram, from neutral and reducing solutions in the lower-right (evolved fluids within layered deposits of basaltic composition) to very acidic and oxidative solutions in the upper-left (concentrated acid sulfate solutions exposed to the atmosphere).

transport toward local topographic lows such as pits at the bottom of NL depressions could have further favored a more rapid thickening of the layered deposits we observed. The layered ash deposits, mostly made of basaltic glass, would have been readily altered by interaction with liquid water, thereby erasing their spectral signature. Ash deposits are favored because a small particle size such as expected for such deposits is consistent with the alteration and erosion observed. However, we do not exclude deposition of eolian sediments from other sources, understanding that they also would be of fine size and roughly basaltic composition, as is the case for most primary materials on Mars, and thus would not confer a substantial initial heterogeneity to the deposits. Still, small variations in initial composition could have influenced the mineralogy ultimately formed by the alteration.

[71] Precipitation of the observed deposits out of solution is a challenging hypothesis. It would require, to form smectite layers, a sustained alkaline body of water with continuous input of fluids of rather constant composition (yielding precipitation of mostly Fe-smectite) counteracting evaporation, and either originally 300 m deep or involving either a rising water table or subsiding floor. First, we noted that no evidence of a lake has been found. Then, this process would not account for the decreasing signature of hydrous minerals upward in the stratigraphy. Thus, we restrict the second process, precipitation of minerals out of solution, to the formation of relatively thin strata and pore-filling cements within pre-existing deposits.

[72] We suggest that the current limited extent of the deposits results from selective induration and armoring by processes limited to the lowest pits, that will be addressed later, while potential surrounding deposits would have been eroded away.

6.1.2. Origin of Volatiles: Water and Sulfur

[73] Aqueous minerals require liquid water to form. In the Late Hesperian or subsequent epochs, two distinct settings of liquid water input may be considered: (1) runoff from melting of snow deposits and (2) groundwater.

[74] Late Hesperian fluvial activity, including branching valleys, has been observed by *Mangold et al.* [2008a] on Valles Marineris (VM) plateau near Echus and Juventae Chasmata. These valleys cut through a thin dark unit topping the plateau. Within this unit, and close to these valleys and to VM sapping canyons, hydrated layers bearing opaline silica and Fe-sulfates have been identified by *Milliken et al.* [2008]. The source of water in this region could have been snow deposition, which is predicted at high obliquity by climate models [*Laskar et al.*, 2004; *Forget et al.*, 2006; *Madeleine et al.*, 2009]. For instance, *Madeleine et al.* [2009, Figure 7] show that snow deposition may have occurred in the western Valles Marineris area (encompassing the depression studied in this paper), in agreement with putative relics of glacial landforms in East Noctis Labyrinthus or Ius Chasma [*Mège and Bourgeois*, 2010]. Snowmelt in specific conditions could have promoted runoff and alteration. However, runoff morphologies have not been observed in the depression, and weathering from intermittent runoff at low temperature likely would have been too slow to form hydrous minerals. Considering also the constraint of different atmospheric conditions than the current ones to support surface runoff, we favor groundwater circulation for alteration of the layered deposits. Assuming the presence of a regional ground-ice reservoir below Tharsis [*Andrews-Hanna et al.*, 2007], high heat flux resulting from regional heat flux and/or magmatic activity would have promoted thawing of subsurface ground-ice and/or snow deposits, and circulation of groundwater. The inner pit, with its low elevation within a ~4 km deep depression, could have focused local seepage, locally providing liquid water toward the pit and promoting alteration of ash deposits and bedrock there. A sustained output of water at the surface by seepage would have formed amphitheater heads, which were not observed. Thus, morphological evidence cannot help us define a stable water table level. Accordingly, it is likely that the actual level of the water table varied with time and was mostly confined at or below the level of the layered deposits.

[75] The pervasive character of Fe-sulfates in the pit requires a significant enrichment in sulfur-rich species from a basaltic composition, a trend also observed at the Viking, Pathfinder and MER landing sites [see *Chevrier and Mathe*, 2007, and references therein]. On the basis of the sulfur enrichment in the Martian soil, acid sulfate alteration has long been considered as a pervasive process on Mars. For instance, *Tosca et al.* [2004] allowed synthetic Martian basalt analogs to alter for 2 weeks at 25°C in acid sulfate solutions of various concentrations, forming Fe oxides from low concentration (i.e., mildly acidic) solutions and several Ca, Mg and Fe sulfates from more acidic solutions. Thus, the presence of Fe-sulfates in the pit is the likely signature of the interaction of primary basaltic material with acid sulfate waters. Sulfur gases, mainly SO_2 on Mars [*Gaillard and Scaillet*, 2009], released by magmatic activity would form sulfuric acid when interacting with oxidizing near-surface waters following the reaction:

$$SO_2 + \frac{1}{2}O_2 + H_2O \rightarrow H_2SO_4 \quad (1)$$

Alternatively, sulfides present at depth such as pyrite (FeS_2) or pyrrhotite ($Fe_{1-x}S$), interacting with hydrothermal water, would locally generate acid sulfate solutions [*Chevrier et al.*, 2004; *Dehouck et al.*, 2011].

6.1.3. Cold Versus Epithermal Environment

[76] On Earth, alteration of basaltic glass in low temperature (0–20°C) environments typically results in authigenic minerals which can be allophane, smectites, kaolinite, gibbsite, or opaline silica depending on the amount of rainfall and soil pH [e.g., *Hay and Iijima*, 1968; *Hay and Jones*, 1972; *Silber et al.*, 1994; *Schiffman et al.*, 2000]. In settings where hydrothermal activity promotes emission of steam then passing through tephra deposits, palagonitization occurs, forming palagonite, a leached hydrated glass with pore-filling zeolites and calcite [*Schiffman et al.*, 2000]. Studies of tuff alteration from Japan, Israel, New Zealand and Hawaii suggests that the annual input of water strongly controls the main weathering products: smectite formation appears to be limited to low rainfall settings (<50 cm/yr) while kaolinite and allophane minerals form in neutral soils under high precipitations (85–300 cm/yr) [see *Silber et al.*, 1994, and references therein; *Schiffman et al.*, 2000]. In Hawaii, downwind of Kilauea, opaline crusts dominate due to complete dissolution of surficial glass at the lower pH (3.5–6) generated by acidic aerosols fallout.

[77] It thus appears that low temperature pedogenic weathering could have formed some of the phases we observed (opaline silica, kaolinite-group minerals, smectites) with variable liquid water input and acidity. However, in the epochs considered (Late Hesperian and later), occasional seepage of groundwater in a cold surface environment would likely not yield water to rock ratios high enough to compare with settings of formation of kaolin-group minerals on Earth. Furthermore, low temperature (e.g., 0–20°C) environments are challenging because of the kinetics, first of glass dissolution (2 orders of magnitude slower at 0°C compared to 100°C according to *Gislason and Oelkers* [2003, Figure 9]), and particularly kinetics of formation of some observed phases, especially Fe-smectite, as experimental alteration relevant to terrestrial settings show. For instance, alteration of tholeiitic glass in fresh and seawater at 20°C showed no alteration for 10 months (after 14 months, a few μm thick palagonitized layer had formed) [*Furnes*, 1975]. Also, alteration by *Cuadros et al.* [1999] of a smectite-free volcanic tuff at already high temperature (~82°C), and for more than 100 days, did not form smectite. For Martian environments, a rare estimate of clay formation times has been reported by *Browning et al.* [2003]: at cold temperatures (5°C), for ash-sized (tens of μm) grains, formation of detectable clay deposits would take on the order of years (compared to hours at 100°C). In a cold environment, considering the likely limited temporal availability of liquid water (e.g., a few days per Martian year), the formation of Fe-smectite in tens of meters thick deposits could have taken thousands to millions of years. If such a cold environment allowed formation of the quantity of phyllosilicates observed in the pit studied, we believe that phyllosilicate outcrops from the Late Hesperian and later should be much more frequent. We thus do not favor a cold surface environment here.

[78] On the contrary, the observed diversity of aqueous minerals is more likely to have formed from the shallow circulation of warm acid-sulfate waters overlying a deeper hydrothermal system. Temperatures in the 50–100°C range would meet the kinetic (phyllosilicate formation) and thermodynamic (no phases typical of high temperatures, such as chlorite) constrains. Interestingly, a batch of epithermal (75°C) acid-sulfate alteration experiments on a synthetic Martian basalt generated a mineral assemblage (Fe-oxi/hydroxides, Fe-sulfates and amorphous silica) comparable to the one we observed (though lacking phyllosilicates, likely due to their slow formation kinetics) [*Hurowitz et al.*, 2005]. Comparison of our observations with this experimental result argues for an acid sulfate hydrothermal setting in the pit studied. Also supportive of this conclusion are the facts that on Earth, halloysite has been found in relation to acid sulfate waters (geothermal or cold meteoric waters affected by pyrite oxidation) [*Ece et al.*, 2008; *Keller and Hanson*, 1968, 1969; *Perruchot et al.*, 1997], and that the Fe-smectite nontronite has been shown to form from hydrothermal alteration of Fe-rich silicates, including active hydrothermal systems on the seafloor [see *Keeling et al.*, 2000, and references therein].

[79] In the envisioned geologic setting, warm acidic groundwater, driven by thermal convection, would circulate within the bedrock and layered deposits through fractures (such as those observed in the Fe-sulfate and Fe-smectite bearing units) and would promote acid dissolution of the bedrock and layered deposits. At shallow depth, warm temperatures and persistent solutions would promote formation of phyllosilicates. At the surface, fluids would be exposed to cold and arid conditions, and evaporation/freezing would concentrate the solutions, promoting precipitation of Fe-sulfates. This setting would be similar to terrestrial active hydrothermal systems with hot springs and fumaroles. Interestingly, the scattered patches of sulfates described in section 5.2.5 could represent sulfate mineralization around hydrothermal vents, consistent with this hypothesis.

6.2. Alteration of Layered Deposits to Fe-Sulfates and Fe-Smectite

6.2.1. The Origin of Fe-Sulfates in the Main Fe-Sulfates Unit

[80] We observed in the lower ~40 m of layered deposits a continuous unit with Fe-sulfates in various hydration states. The possible eolian bed forms identified on the sulfate unit are consistent with eolian mobilization of material first, and its later alteration into sulfates, as observed in Meridiani Planum [*Arvidson et al.*, 2006a; *Squyres et al.*, 2006] and postulated for other depressions of Valles Marineris [e.g., *Mangold et al.*, 2008b; *Murchie et al.*, 2009a]. In the setting considered, layered basaltic ashes (i.e., tuff deposits), were altered by hot acid sulfate waters. Assuming input of hot acid sulfate solutions at the bottom of the pit, alteration would have been maximal for the earlier, lower layered deposits and gradually less for later, upper deposits.

[81] Acid sulfate solutions circulating through tuff deposits of basaltic composition would have dissolved Na^{+}, K^{+}, Ca^{2+}, Mg^{2+}, Al^{3+}, Fe^{2+} and would have become enriched in these cations, as well as in Fe^{3+}, formed by oxidation in contact with atmospheric conditions. Continuous supply of fluids at the bottom of the pit would have maintained very acidic conditions. At the surface, exposed to cold and arid conditions, evaporation and/or freezing of solutions would have occurred, concentrating solutes and eventually leading to the precipitation of various Fe-sulfates such as szomolnokite ($Fe^{II}SO_4.H_2O$) or coquimbite ($Fe_2^{III}(SO_4)_3.9H_2O$). The ~40 m of the main Fe-sulfates unit would have been constructed by either a single large tuff deposition and acid sulfate alteration event, or repeated sequences of deposition and alteration of layers.

6.2.2. Fe-Smectite Origin in an Acid Hydrothermal Setting

[82] Attempts of experimental Fe-smectite synthesis in neutral to acidic conditions are scarce in the literature. *Harder* [1976] synthesized nontronite from Fe and silica rich solutions at pH ~ 7–10, and showed that partially reducing conditions favored rapid Fe-smectite formation (a few days) at the expense of Fe-oxi/hydroxides. In more oxidizing conditions, synthesis of nontronite is effective in more alkaline conditions (pH ~ 12 [*Decarreau et al.*, 2008]). We examine in this section how the neutral and reducing conditions required for Fe-smectite formation could be attained in the acid hydrothermal setting considered thus far.

[83] Considering that recognized Martian basalts show redox conditions from QFM-3.5 to QFM-1 (QFM being the Quartz-Fayalite-Magnetite oxygen fugacity buffer) [*Gaillard and Scaillet*, 2009], i.e., close to the reducing dissociation of water, the volcanic ashes forming the deposits likely had a

reduced composition which, isolated from the oxidizing atmosphere, favored reducing conditions within the deposits.

[84] We assume a mean level of the water table of hydrothermal solutions near the upper limit of the main Fe-sulfates unit. Above this level, renewal of acidity would have been low, with input of solutions mostly from slow percolation through the deposits, allowing solutions to evolve toward neutral conditions by cation exchange. Indeed, acidic dissolution of basaltic glass proceeds by replacement of cations M of a given charge n by an equivalent number of protons, buffering the acidity of the solution according to the equilibrium:

$$M_{glass} + nH^+ \rightarrow M^{n+} + H_{glass} \quad (2)$$

On the surfaces of glass elements, these evolved, mildly acidic solutions would first take-up modifying glass elements such as Na, K, Ca, Mg while constitutive Si, Al and oxidized Fe^{III} would remain in the leached surficial glass framework, forming the precursor of neoformed clays [see *Oelkers and Gislason*, 2001, and references therein]. Consequently, near-neutral pH and partly reducing hot (50–100°C) fluids, persisting for at least a few days, would have favored neoformation of Fe-smectite from Fe and silica rich glass surfaces.

[85] If the fluids reached the surface, where oxidizing conditions of the atmosphere prevailed, precipitation of Fe-oxi/hydroxides such as goethite (FeOOH) or ferrihydrite (Fe_2O_3. $1/2H_2O$) would have been favored. Either in this form or transformed to hematite Fe_2O_3 by later dehydration, these minerals could account for the Fe-oxi/hydroxides signatures in the Fe-smectite unit.

6.2.3. Formation of Interbedded Fe-Sulfates

[86] The coexistence of Fe-smectite, forming at neutral pH, and jarosite, forming at pH $\sim$ 1–4, is unusual, but not implausible. Indeed, *Altheide et al.* [2010] conducted experimental acid weathering of phyllosilicates at various pHs: the Fe-smectite was spectrally unchanged at pH 4 but disappeared at pH 2 and 0. Thus, formation of jarosite at pH $\sim$ 3–4 would have been possible without obliterating Fe-smectite signatures.

[87] The raise in acidity needed to allow jarosite precipitation could have been provided by transient rises of the water table or arrival of acid fluids through faults and fractures, forming scattered vents within the deposits, as tentatively identified in the observed patches of Fe-sulfates (section 5.2.5). Acid sulfate solutions would have begun to alter the Fe-smectite at the surface while evaporation and/or freezing would have promoted precipitation of jarosite (9):

$$K^+/Na^+ + 3Fe^{3+} + 2SO_4{}^{2-} + 6H_2O \rightarrow (K/Na)Fe_3(SO_4)_2(OH)_6 + 6H^+ \quad (3)$$

This reaction tends to increase the acidity of the solution, which would increase Fe-smectite dissolution, but high aridity and low fluid input would have stopped the process by removing the liquid water.

6.2.4. Fate of the Missing, Leached Cations

[88] Na, Ca and Mg each make up several percent of typical Martian basalts in oxide weight. We did not observe a unit dominated by Na, Ca or Mg rich phases such as Ca- and Mg- sulfates, or Mg-smectite. However, anhydrous sulfates, such as anhydrite ($CaSO_4$), are spectrally bland [*Cloutis et al.*, 2006], and could be present within other units, e.g., mixed with Fe-smectite or Fe-sulfates. The presence of several percent of monohydrated Mg-sulfate in the main Fe-sulfates unit is also consistent with CRISM spectra of this unit, as described in section 4.2, and could account for some of the Mg. Also, the Fe-smectite unit could in fact retain some Mg substituted for Fe in the smectite octahedral sites. Finally, most of the Na could have been taken up by the precipitation of (natro-)jarosite.

[89] Alternatively, leaching solutions of layered deposits alteration, enriched in Na, Ca and Mg could have percolated downward through the layered deposits and into the bedrock.

6.3. Alteration of the Bedrock to Halloysite and Hydrated Silica

[90] Stratigraphically below all layered units, the bedrock of the "proto" pit existed at the bottom of the depression before emplacement of the layered deposits. Probably originally of basaltic composition, it now bears two different mineralogies at its top: halloysite (H unit) and hydrated silica (Si unit). Unit H is found at lowest elevations, at the bottom and center of the pit, while unit Si is present on the walls of the pit, at its periphery and at higher elevations than H. In addition, we noted that the Si unit bears Fe-oxi/hydroxides signatures. Formation of both halloysite and hydrated amorphous silica implies processes of Si and Al selective concentration relative to other elements, and therefore intense leaching. Candidate settings include pedogenetic weathering, or groundwater circulation. We then show that a pedogenetic setting was unlikely (1), and then examine how in a groundwater fed system, selective dissolution of primary materials (2) and/or precipitation (3) could have formed both minerals.

6.3.1. The Pedogenetic Hypothesis

[91] Halloysite/kaolinite is often interpreted as resulting from pedogenesis on Earth (in semi-arid conditions in Israel [*Silber et al.*, 1994] and in Australia [*Eggleton et al.*, 1987], or in arid conditions with intense short wet periods in Hawaii [*Ziegler et al.*, 2003]). However, it can also be hydrothermal [e.g., *Ece et al.*, 2008]. On Mars, kaolinite (analog to halloysite) has been found in different locations: at Mawrth Vallis [*Loizeau et al.*, 2010; *Bishop et al.*, 2008a; *Wray et al.*, 2008] and Nili Fossae [*Ehlmann et al.*, 2009; *Gaudin et al.*, 2011], and is suspected to correspond to a pedogenetic environment. However, the kaolinite layer there is consistently present at the top of an alteration column, and associated with larger smectites outcrops, which are also expected to form under pedogenetic processes [*Gaudin et al.*, 2011]. In contrast, we did not observe smectites in the bedrock unit. In addition, the halloysite unit only outcrops at depth: the same bedrock does not show any kaolinite or halloysite at the top of the pit, neither elsewhere outside of the pit (i.e., on the surface of the depression). Thus, considering the absence of smectite in the bedrock, the presence of halloysite at strong depth and its absence elsewhere but the bottom of the pit, alteration of the bedrock is much more consistent with local groundwater circulation than with extensive weathering.

6.3.2. Non-Selective Dissolution of Primary Basaltic Material

[92] The formation of amorphous silica in the Si unit and halloysite in the H unit could be explained by distinct original compositions, such as presence or absence of olivine [*Tosca et al.*, 2004]. Indeed, the susceptibility of constituents of basalt to typical low acid to neutral weathering on Earth is different, with, from most readily altered to most stable: glass and olivine, plagioclase, pyroxene, oxides [e.g., *Eggleton et al.*, 1987]. We consider this trend although for very acidic conditions the susceptibility of basaltic minerals to alteration may be slightly different (faster clinopyroxene (HCP) dissolution at 0°C and pH < ~3–4 reported by *McAdam et al.* [2008], oxides and plagioclase feldspar dissolution before clinopyroxene at pH ~ 1 and ~70°C reported by *Hurowitz et al.* [2005]). In olivine-free basalt, rapid alteration of plagioclase can allow neoformation of Al-rich clays, such as kaolinite/halloysite. For an olivine basalt, acid sulfate alteration first releases abundant Si from olivine dissolution, and amorphous silica can precipitate in aggregates on the basalt surface [*Tosca et al.*, 2004]. However, we do not favor the hypothesis of distinct olivine contents, as we did not identify olivine anywhere in the depression studied, nor the Mg-rich phases that would likely result from Mg leached by olivine.

6.3.3. Selective Precipitation of Hydrated Silica and Halloysite at Various pH

[93] If selective dissolution of varying minerals was not a driving factor, selective precipitation of amorphous silica or halloysite from the same Si and Al rich solution may have been favored by different conditions because of the different behavior of Si and Al solubilities.

[94] Silicic acid solubility at pH < 9 is independent of pH but depends on temperature, being three times less at 0°C (~$10^{-2.7}$) than at 100°C [*Siever*, 1962]. On the contrary, Al solubility is minimal in near neutral conditions (~10^{-12} M at pH ~ 6) and increases by several orders of magnitude in acidic conditions (~10^{-2} at pH ~ 2) [*Hurowitz et al.*, 2006]. *Hurowitz et al.* [2005] showed that when basalt was attacked by a pH ~ 1 solution, amorphous silica precipitated as a residual when undergoing a sudden drop in temperature; conversely, in a pH ~ 5 solution, precipitation of clays such as kaolinite was expected, although not observed due to the short duration of their experiments relative to kaolinite formation kinetics.

[95] A comparable process could have occurred in the studied area, assuming a hydrothermal system centered at the pit, with high temperature (>100°C) acid sulfate solutions circulating through faults and fractures, reaching the surface at the periphery as well as at the center of the pit. Minerals such as plagioclase and HCP would have been dissolved, releasing Ca, Na, Fe, Al and Si in solution, following reactions (2) to (4):

$$\text{Ca}-\text{pl.}\quad \mathrm{CaAl_2Si_2O_8} + 8\mathrm{H^+} \rightarrow \mathrm{Ca^{2+}} + 2\mathrm{Al^{3+}} + 2\mathrm{SiO_2} + 4\mathrm{H_2O} \tag{4}$$

$$\text{Na}-\text{pl.}\quad \mathrm{NaAlSi_3O_8} + 4\mathrm{H^+} \rightarrow \mathrm{Na^+} + \mathrm{Al^{3+}} + 3\mathrm{SiO_2} + 2\mathrm{H_2O} \tag{5}$$

$$\text{HCP}\quad \mathrm{(Ca,Mg,Fe)SiO_3} + 2\mathrm{H^+} \rightarrow \mathrm{Ca^{2+}/Mg^{2+}/Fe^{2+}} + \mathrm{SiO_2} + \mathrm{H_2O} \tag{6}$$

with also partial oxidation of Fe^{2+} to Fe^{3+}:

$$\mathrm{Fe^{2+}} + \frac{1}{4}\mathrm{O_2} + \mathrm{H^+} \rightarrow \mathrm{Fe^{3+}} + \frac{1}{2}\mathrm{H_2O} \tag{7}$$

It can be noted here that these dissolution reactions consume acidity, thereby increasing the pH of the alteration solution. However, in a flow-through regime, such as on the slopes of the walls of the pit studied, renewal of attack solutions and downward flow of leaching solutions would have maintained a low pH, preventing precipitation of Al-clays. Notwithstanding, silica present in the leaching solutions, reaching the colder (~0°C) surface environment, could have precipitated due to the lower solubility of silica at lower temperatures.

[96] On the contrary, toward the center of the pit, input of evolved solutions from the periphery and relatively long persistence of hydrothermal solutions through ponding, increasing interaction with primary material, would have lowered the pH to the stability field of Al-rich clays kaolinite/halloysite (pH ~ 3–6). Higher temperatures would also have favored silica in solution. Alteration of plagioclase in basalt by these more advanced solutions would have formed kaolin-group minerals, following the reactions (6) and (7):

$$\mathrm{CaAl_2Si_2O_8} + \mathrm{H_2O} + 2\mathrm{H^+} \rightarrow \mathrm{Ca^{2+}} + \mathrm{Al_2Si_2O_5(OH)_4} \tag{8}$$

$$2\mathrm{NaAlSi_3O_8} + \mathrm{H_2O} + 2\mathrm{H^+} \rightarrow 2\mathrm{Na^+} + \mathrm{Al_2Si_2O_5(OH)_4} + 4\mathrm{SiO_2} \tag{9}$$

To explain the Fe oxides/hydroxides/oxihydroxides signature of the Si-OH unit in this setting, the hypothesis of a lag deposit remaining after erosion of the Fe-smectite unit is compatible and is consistent with these signatures spanning both units with no discontinuity.

[97] To sum up, selective precipitation of amorphous silica in acidic conditions and halloysite in low acidity conditions are our preferred explanation for the observed mineralogy of the bedrock unit. This process implies input of hot acid sulfate fluids from the periphery and center of the pit, and a downward gradient of increasingly buffered solutions.

6.4. Summary and Sequence of Events

[98] From the processes discussed so far, we can draw a scenario compatible with our observations.

[99] On a basaltic terrain, hot hydrothermal acid sulfate solutions at low pH, would have dissolved plagioclase and HCP, with partial oxidation of Fe^{2+} to Fe^{3+}, and would have reached the surface through faults and fractures on the periphery and floor of a "proto" pit. Dissolution would have consumed acidity, increasing the pH of the alteration solution, and releasing Na, Ca, Al, Fe, Mg and silica in solution. While most solutes would have been leached downward, silica in solution in hot waters would have precipitated when reaching colder areas because of its lower solubility at low temperature. At the bottom of the "proto" pit, with more evolved interaction with the primary material, the pH of the attack solution would have increased, eventually reaching the stability field of Al-rich clays kaolinite/halloysite. At this point, with solutions close to the saturation for these

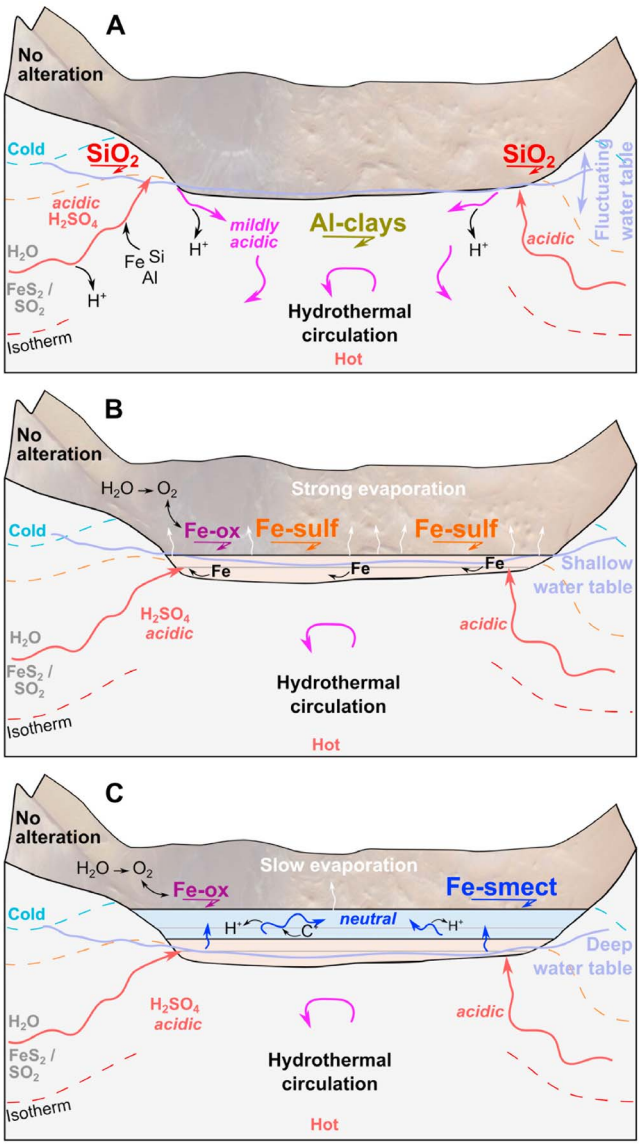

Figure 16. Proposed scenario for the formation of aqueous alteration minerals in the studied pit. (a) Acid sulfate hydrothermal alteration of the bedrock and precipitation of hydrated silica and halloysite. (b) Acid sulfate hydrothermal alteration of air fall layered deposits forming Fe-sulfates. (c) Formation of Fe-smectite within layered deposits due to circulation of confined evolved hydrothermal solutions at low water-to-rock ratio.

minerals, alteration of plagioclase in basalt would have formed kaolin minerals (Figure 16a).

[100] At the bottom of the pit, leachate solutions would have interacted with layered tuffs and their eolian rework being episodically deposited. Within the lowest layers, below the water table, acid sulfate alteration would have completely dissolved the primary glass, forming concentrated solutions. Upon arid conditions (freezing and/or evaporation) at the surface, Fe-sulfates would have precipitated, starting with jarosite (9), driving the pH even lower, and eventually allowing precipitation of hydrated Fe-sulfates such as copiapite or coquimbite. The occurrence of transient lakes at this stage is possible but not necessary (Figure 16b).

[101] At some time, layered deposits from ashes and eolian material would have filled the pit up to above the water table, preventing massive alteration by acid sulfate solutions. However, with solutions slowly percolating through the deposits, alteration would still have occurred, though at low water-to-rock ratio, thereby lowering acidity to neutral conditions through cation exchange and eventually forming Fe-smectites (Figure 16c). During transient periods of higher level of the water table and/or close to scattered hydrothermal vents, locally stronger circulation of acid sulfate fluids and evaporation at the surface would have favored precipitation of Fe(OH) sulfates such as jarosite. As the thickness of deposits would have increased further, and/or hydrothermal activity receded, less alteration would have taken place, leaving diagnostic hydrated minerals in decreasing amounts, or with lower crystallinity, yielding fainter spectral signatures.

[102] This activity would have ceased as the proto pit was filled with deposits. Subsequent modifications would have included superposition of mass-wasting deposits from the walls of the depression and deformation of near-surface layers. Finally, erosion, probably due to katabatic winds converging at the lowest elevation of the depression, would have removed progressively the uppermost weakest material, except where armored by mass-wasting deposits, and exhumed the lowermost hydrated deposits and bedrock.

7. Conclusion

[103] A very diverse assemblage of hydrated minerals has been identified in a pit within one NL depression. Formation of these hydrated minerals was in situ and must have occurred after formation of the depression, i.e., during or after the Late-Hesperian, and thus after the "early Mars" era when most aqueous minerals are thought to have formed. *Weitz et al.* [2011] concluded from the superposition of younger Fe/Mg smectites over sulfates, Al clays and hydrated silica that this region is unique relative to most other locations on Mars where the opposite progression is observed and the Fe/Mg smectites are Noachian.

[104] A detailed analysis of the morphology, composition and stratigraphy of these materials allows us to develop this preliminary conclusion. Our analysis confirms that groundwater-fed hydrothermal alteration is favored as the main alteration trigger but reveals that layered deposits contain interbedded Fe-smectites and Fe-sulfates, with a variety of hydrated and dehydrated sulfates including local jarosite outcrops. Thus, the observed sequence may not represent an opposite progression to the usual sequence (sulfates over smectites) as initially proposed by *Weitz et al.* [2011], but a single environment of formation with local variations in alteration conditions. Variable evaporation and/or freezing rates of leaching solutions reaching the near surface would have controlled the precipitation of various Fe-sulfates. Dissolution of primary minerals buffering the acid attack solutions would have increased the pH of leaching fluids, explaining clay formation in the same context and period as that of sulfates. These processes can account for the coeval formation of Si-OH bearing material and halloysite in the bedrock (acid and mildly acid conditions, respectively), and for the Fe-smectite and Fe-sulfates in the layered deposits

(buffered, long standing, and evaporating acid solutions, respectively).

[105] Our scenario of formation for these minerals does not require global conditions but regional hydrothermalism only, even in a cold Mars surface environment. We infer that comparable local processes may be relevant to other Martian localities with hydrated minerals in local environments with heat sources such as volcanoes and impact craters. Thus, the identification of phyllosilicates is not, by itself, an evidence for an ancient global alteration, but should be carefully coupled to the presence of other alteration minerals and a detailed geological context for a proper conclusion.

[106] **Acknowledgments.** This research benefited from financial supports of the Centre National d'Etudes Spatiales (CNES), the Agence Nationale de la Recherche under grant ANR-08-JCJC-0126 "MADMACS," and the Programme National de Planétologie (PNP) of Institut National des Sciences de l'Univers (INSU-CNRS). We thank K. Lichtenberg and an anonymous reviewer for their insightful comments.

References

Altheide, T. S., et al. (2010), Mineralogical characterization of acid weathered phyllosilicates with implications for secondary Martian deposits, *Geochim. Cosmochim. Acta*, *74*(21), 6232–6248, doi:10.1016/j.gca.2010.08.005.

Anderson, J. H., Jr., and K. A. Wickersheim (1964), Near infrared characterization of water and hydroxyl groups on silica surfaces, *Surf. Sci.*, *2*, 252–260, doi:10.1016/0039-6028(64)90064-0.

Andrews-Hanna, J. C., et al. (2007), Meridiani Planum and the global hydrology of Mars, *Nature*, *446*(7132), 163–166, doi:10.1038/nature05594.

Ansan, V., et al. (2008), Topography of valley networks on Mars from Mars Express High Resolution Stereo Camera digital elevation models, *J. Geophys. Res.*, *113*, E07006, doi:10.1029/2007JE002986.

Arvidson, R. E., et al. (2006a), Nature and origin of the hematite-bearing plains of Terra Meridiani based on analyses of orbital and Mars Exploration rover data sets, *J. Geophys. Res.*, *111*, E12S08, doi:10.1029/2006JE002728.

Arvidson, R. E., et al. (2006b), Overview of the Spirit Mars Exploration Rover Mission to Gusev Crater: Landing site to Backstay Rock in the Columbia Hills, *J. Geophys. Res.*, *111*, E02S01, doi:10.1029/2005JE002499.

Baptista, A. R., et al. (2008), A swarm of small shield volcanoes on Syria Planum, Mars, *J. Geophys. Res.*, *113*, E09010, doi:10.1029/2007JE002945.

Baratoux, D., et al. (2011), Thermal history of Mars inferred from orbital geochemistry of volcanic provinces, *Nature*, *472*(7343), 338–341, doi:10.1038/nature09903.

Bibring, J. P., et al. (2005), Mars surface diversity as revealed by the OMEGA/Mars Express observations, *Science*, *307*(5715), 1576–1581, doi:10.1126/science.1108806.

Bibring, J. P., et al. (2006), Global mineralogical and aqueous mars history derived from OMEGA/Mars express data, *Science*, *312*(5772), 400–404, doi:10.1126/science.1122659.

Bishop, J. L., et al. (2008a), Phyllosilicate diversity and past aqueous activity revealed at Mawrth Vallis, Mars, *Science*, *321*(5890), 830–833, doi:10.1126/science.1159699.

Bishop, J. L., et al. (2008b), Reflectance and emission spectroscopy study of four groups of phyllosilicates: Smectites, kaolinite-serpentines, chlorites and micas, *Clay Miner.*, *43*(1), 35–54, doi:10.1180/claymin.2008.043.1.03.

Bishop, J. L., et al. (2009), Mineralogy of Juventae Chasma: Sulfates in the light-toned mounds, mafic minerals in the bedrock, and hydrated silica and hydroxylated ferric sulfate on the plateau, *J. Geophys. Res.*, *114*, E00D09, doi:10.1029/2009JE003352. [Printed *115*(E2), 2010].

Brown, J. B. (1971), Jarosite-geoethite stabilities at 25°C, 1 ATM, *Miner. Deposita*, *6*(3), 245–252, doi:10.1007/BF00208032.

Browning, L., et al. (2003), Minimum times to form clay in Martian surface and near-surface environments, *Lunar Planet. Sci.*, *XXXIV*, Abstract 1708.

Burns, R. G. (1987), Ferric sulfates on Mars, *J. Geophys. Res.*, *92*(B4), E570–E574, doi:10.1029/JB092iB04p0E570.

Cariati, F., et al. (1981), Water molecules and hydroxyl groups in montmorillonites as studied by near infrared spectroscopy, *Clays Clay Miner.*, *29*(2), 157–159, doi:10.1346/CCMN.1981.0290211.

Chevrier, V., and P. E. Mathe (2007), Mineralogy and evolution of the surface of Mars: A review, *Planet. Space Sci.*, *55*(3), 289–314, doi:10.1016/j.pss.2006.05.039.

Chevrier, V., et al. (2004), Weathering of iron-rich phases in simulated Martian atmospheres, *Geology*, *32*(12), 1033–1036, doi:10.1130/G21078.1.

Christensen, P. R., et al. (2000), Detection of crystalline hematite mineralization on Mars by the Thermal Emission Spectrometer: Evidence for near-surface water, *J. Geophys. Res.*, *105*(E4), 9623–9642, doi:10.1029/1999JE001093.

Christiansen, R. L. (2001), The Quaternary and Pliocene Yellowstone Plateau Volcanic Field of Wyoming, Idaho, and Montana, *U. S. Geol. Surv. Prof. Pap.*, *729-G*, 120 pp.

Clark, R. N., et al. (1990), High spectral resolution reflectance spectroscopy of minerals, *J. Geophys. Res.*, *95*(B8), 12,653–12,680, doi:10.1029/JB095iB08p12653.

Clark, R. N., G. A. Swayze, R. Wise, E. Livo, T. Hoefen, R. Kokaly, and S. J. Sutley (2007), USGS digital spectral library splib06a, *U.S. Geol. Surv. Digital Data Ser. 231*, report, U.S. Geol. Surv., Denver, Colo. [Available at http://speclab.cr.usgs.gov/spectral.lib06].

Cloutis, E. A., et al. (2006), Detection and discrimination of sulfate minerals using reflectance spectroscopy, *Icarus*, *184*(1), 121–157, doi:10.1016/j.icarus.2006.04.003.

Cuadros, J., et al. (1999), Experimental alteration of volcanic tuff; smectite formation and effect on ^{18}O isotope composition, *Clays Clay Miner.*, *47*(6), 769–776, doi:10.1346/CCMN.1999.0470612.

Decarreau, A., et al. (2008), Hydrothermal synthesis, between 75 and 150°C, of high-charge, ferric nontronites, *Clays Clay Miner.*, *56*(3), 322–337, doi:10.1346/CCMN.2008.0560303.

Dehouck, E., et al. (2011), Role of sulfide-weathering in the formation of sulfates or carbonates on Mars, *Lunar Planet. Sci.*, *XLII*, Abstract 1715.

Dyar, M. D., et al. (2005), MIL03346, the most oxidized Martian meteorite: A first look at spectroscopy, petrography, and mineral chemistry, *J. Geophys. Res.*, *110*, E09005, doi:10.1029/2005JE002426.

Eberl, D. D., et al. (1984), Clay mineral formation and transformation in rocks and soils (and discussion), *Philos. Trans. R. Soc. London A*, *311*(1517), 241–257.

Ece, O. I., et al. (2008), Acid-sulphate hydrothermal alteration of andesitic tuffs and genesis of halloysite and alunite deposits in the Biga Peninsula, Turkey, *Clay Miner.*, *43*(2), 281–315, doi:10.1180/claymin.2008.043.2.10.

Eggleton, R. A., et al. (1987), Weathering of basalt: Changes in rock chemistry and mineralogy, *Clays Clay Miner.*, *35*(3), 161–169, doi:10.1346/CCMN.1987.0350301.

Ehlmann, B. L., et al. (2008), Orbital identification of carbonate-bearing rocks on Mars, *Science*, *322*(5909), 1828–1832, doi:10.1126/science.1164759.

Ehlmann, B. L., et al. (2009), Identification of hydrated silicate minerals on Mars using MRO-CRISM: Geologic context near Nili Fossae and implications for aqueous alteration, *J. Geophys. Res.*, *114*, E00D08, doi:10.1029/2009JE003339. [Printed *115*(E2), 2010].

Forget, F., et al. (2006), Formation of glaciers on Mars by atmospheric precipitation at high obliquity, *Science*, *311*(5759), 368–371, doi:10.1126/science.1120335.

Furnes, H. (1975), Experimental palagonitization of basaltic glasses of varied composition, *Contrib. Mineral. Petrol.*, *50*(2), 105–113, doi:10.1007/BF00373330.

Gaidos, E., and G. Marion (2003), Geological and geochemical legacy of a cold early Mars, *J. Geophys. Res.*, *108*(E6), 5055, doi:10.1029/2002JE002000.

Gaillard, F., and B. Scaillet (2009), The sulfur content of volcanic gases on Mars, *Earth Planet. Sci. Lett.*, *279*(1–2), 34–43, doi:10.1016/j.epsl.2008.12.028.

Garrels, R. M., and C. L. Christ (1965), *Solutions, Minerals, and Equilibria*, 450 pp., Harper and Row, New York.

Gaudin, A., et al. (2011), Evidence for weathering on early Mars from a comparison with terrestrial weathering profiles, *Icarus*, *216*(1), 257–268.

Gendrin, A., et al. (2005), Sulfates in Martian layered terrains: The OMEGA/Mars Express view, *Science*, *307*(5715), 1587–1591, doi:10.1126/science.1109087.

Gislason, S. R., and E. H. Oelkers (2003), Mechanism, rates, and consequences of basaltic glass dissolution: II. An experimental study of the dissolution rates of basaltic glass as a function of pH and temperature, *Geochim. Cosmochim. Acta*, *67*(20), 3817–3832, doi:10.1016/S0016-7037(03)00176-5.

Harder, H. (1976), Nontronite synthesis at low temperatures, *Chem. Geol.*, *18*(3), 169–180, doi:10.1016/0009-2541(76)90001-2.

Hartmann, W. K., and G. Neukum (2001), Cratering chronology and the evolution of Mars, *Space Sci. Rev.*, *96*(1), 165–194.

Hay, R. L., and A. Iijima (1968), Petrology of palagonite tuffs of Koko Craters, Oahu, Hawaii, *Contrib. Mineral. Petrol.*, *17*(2), 141–154, doi:10.1007/BF00373206.

Hay, R. L., and B. F. Jones (1972), Weathering of basaltic tephra on the island of Hawaii, *Geol. Soc. Am. Bull.*, *83*(2), 317–332, doi:10.1130/0016-7606(1972)83[317:WOBTOT]2.0.CO;2.

Hurowitz, J. A., et al. (2005), Experimental epithermal alteration of synthetic Los Angeles meteorite: Implications for the origin of Martian soils and identification of hydrothermal sites on Mars, *J. Geophys. Res.*, *110*, E07002, doi:10.1029/2004JE002391.

Hurowitz, J. A., et al. (2006), In situ and experimental evidence for acidic weathering of rocks and soils on Mars, *J. Geophys. Res.*, *111*, E02S19, doi:10.1029/2005JE002515.

Ivanov, B. A. (2001), Mars/Moon cratering rate ratio estimates, *Space Sci. Rev.*, *96*(1), 87–104.

Joussein, E., et al. (2005), Halloysite clay minerals–A review, *Clay Miner.*, *40*(4), 383–426, doi:10.1180/0009855054040180.

Keeling, J. L., et al. (2000), Geology and characterization of two hydrothermal nontronites from weathered metamorphic rocks at the Uley graphite mine, South Australia, *Clays Clay Miner.*, *48*(5), 537–548, doi:10.1346/CCMN.2000.0480506.

Keller, W. D., and R. F. Hanson (1968), Hydrothermal alteration of a rhyolite flow breccia near San Luis Potosi, Mexico, to refractory kaolin, *Clays Clay Miner.*, *16*(3), 223, doi:10.1346/CCMN.1968.0160304.

Keller, W. D., and R. F. Hanson (1969), Hydrothermal argillation of volcanic pipes in limestone in Mexico, *Clays Clay Miner.*, *17*(1), 9, doi:10.1346/CCMN.1969.0170103.

Kerber, L., et al. (2008), The distribution of ash from ancient explosive volcanoes on Mars, paper presented at Vernadsky-Brown Microsymposium 48, Vernadsky Inst. and Brown Univ., Moscow, 20–22 October.

King, P. L., and H. Y. McSween Jr. (2005), Effects of H_2O, pH, and oxidation state on the stability of Fe minerals on Mars, *J. Geophys. Res.*, *110*, E12S10, doi:10.1029/2005JE002482.

Klingelhöfer, G., et al. (2004), Jarosite and hematite at Meridiani Planum from Opportunity's Mössbauer spectrometer, *Science*, *306*(5702), 1740–1745, doi:10.1126/science.1104653.

Laskar, J., et al. (2004), Long term evolution and chaotic diffusion of the insolation quantities of Mars, *Icarus*, *170*(2), 343–364, doi:10.1016/j.icarus.2004.04.005.

Lichtenberg, K. A., et al. (2010), Stratigraphy of hydrated sulfates in the sedimentary deposits of Aram Chaos, Mars, *J. Geophys. Res.*, *115*, E00D17, doi:10.1029/2009JE003353.

Ling, Z. C., and A. Wang (2010), A systematic spectroscopic study of eight hydrous ferric sulfates relevant to Mars, *Icarus*, *209*(2), 422–433, doi:10.1016/j.icarus.2010.05.009.

Loizeau, D., et al. (2010), Stratigraphy in the Mawrth Vallis region through OMEGA, HRSC color imagery and DTM, *Icarus*, *205*(2), 396–418, doi:10.1016/j.icarus.2009.04.018.

Madejová, J., et al. (2009), Near-infrared spectroscopy: A powerful tool in studies of acid-treated clay minerals, *Vibrational Spectrosc.*, *49*(2), 211–218, doi:10.1016/j.vibspec.2008.08.001.

Madeleine, J. B., et al. (2009), Amazonian northern mid-latitude glaciation on Mars: A proposed climate scenario, *Icarus*, *203*(2), 390–405, doi:10.1016/j.icarus.2009.04.037.

Majzlan, J., et al. (2006), Thermodynamic properties and crystal structure refinement of ferricopiapite, coquimbite, rhomboclase, and $Fe_2(SO_4)_3(H_2O)_5$, *Eur. J. Mineral.*, *18*(2), 175–186, doi:10.1127/0935-1221/2006/0018-0175.

Malin, M. C., et al. (2007), Context Camera Investigation on board the Mars Reconnaissance Orbiter, *J. Geophys. Res.*, *112*, E05S04, doi:10.1029/2006JE002808.

Mangold, N., et al. (2008a), Geomorphic study of fluvial landforms on the northern Valles Marineris plateau, Mars, *J. Geophys. Res.*, *113*, E08009, doi:10.1029/2007JE002985.

Mangold, N., et al. (2008b), Spectral and geological study of the sulfate-rich region of West Candor Chasma, Mars, *Icarus*, *194*(2), 519–543, doi:10.1016/j.icarus.2007.10.021.

Mangold, N., et al. (2010a), Mineralogy of recent volcanic plains in the Tharsis region, Mars, and implications for platy-ridged flow composition, *Earth Planet. Sci. Lett.*, *294*(3–4), 440–450, doi:10.1016/j.epsl.2009.07.036.

Mangold, N., et al. (2010b), A Late Amazonian alteration layer related to local volcanism on Mars, *Icarus*, *207*(1), 265–276, doi:10.1016/j.icarus.2009.10.015.

Masson, P. (1980), Contribution to the structural interpretation of the Valles Marineris–Noctis Labyrinthus–Claritas Fossae regions of Mars, *Earth Moon Planets*, *22*(2), 211–219, doi:10.1007/BF00898432.

McAdam, A. C., et al. (2008), Preferential low-pH dissolution of pyroxene in plagioclase-pyroxene mixtures: Implications for Martian surface materials, *Icarus*, *196*(1), 90–96, doi:10.1016/j.icarus.2008.01.008.

McEwen, A. S., et al. (2007), Mars Reconnaissance Orbiter's High Resolution Imaging Science Experiment (HiRISE), *J. Geophys. Res.*, *112*, E05S02, doi:10.1029/2005JE002605.

McKeown, N. K., et al. (2011), Interpretation of reflectance spectra of mixtures of clay mineral-silica mixtures: Implications for Martian clay mineralogy at Mawrth Vallis, *Clays Clay Miner.*, *59*(4), 400–415.

McSween, H. Y., Jr., and A. H. Treiman (1999), Martian meteorites, in *Planetary Materials*, *Rev. Mineral. Geochem.*, vol. 36, pp. 6-01–6-54, edited by J. J. Papike, Mineral. Soc. of Am., Washington, D. C.

Mège, D., and O. Bourgeois (2010), Destabilization of Valles Marineris wallslopes by retreat of ancient glaciers, *Lunar Planet. Sci.*, *XLI*, Abstract 1713.

Mège, D., et al. (2003), Volcanic rifting at Martian grabens, *J. Geophys. Res.*, *108*(E5), 5044, doi:10.1029/2002JE001852.

Michael, G. G., and G. Neukum (2010), Planetary surface dating from crater size-frequency distribution measurements: Partial resurfacing events and statistical age uncertainty, *Earth Planet. Sci. Lett.*, *294*(3–4), 223–229, doi:10.1016/j.epsl.2009.12.041.

Milliken, R. E., et al. (2008), Opaline silica in young deposits on Mars, *Geology*, *36*(11), 847–850, doi:10.1130/G24967A.1.

Milliken, R. E., et al. (2010), Paleoclimate of Mars as captured by the stratigraphic record in Gale Crater, *Geophys. Res. Lett.*, *37*, L04201, doi:10.1029/2009GL041870.

Morris, R. V., et al. (2008), Iron mineralogy and aqueous alteration from Husband Hill through Home Plate at Gusev Crater, Mars: Results from the Mössbauer instrument on the Spirit Mars Exploration Rover, *J. Geophys. Res.*, *113*, E12S42, doi:10.1029/2008JE003201.

Morris, R. V., et al. (2009), Visible and near-IR reflectance spectra for smectite, sulfate and perchlorate under dry conditions for interpretation of Martian surface mineralogy, *Lunar Planet. Sci.*, *XL*, Abstract 2317.

Morris, R. V., et al. (2010), Identification of carbonate-rich outcrops on Mars by the Spirit Rover, *Science*, *329*(5990), 421–424, doi:10.1126/science.1189667.

Murchie, S., et al. (2007), Compact Reconnaissance Imaging Spectrometer for Mars (CRISM) on Mars Reconnaissance Orbiter (MRO), *J. Geophys. Res.*, *112*, E05S03, doi:10.1029/2006JE002682.

Murchie, S., et al. (2009a), Evidence for the origin of layered deposits in Candor Chasma, Mars, from mineral composition and hydrologic modeling, *J. Geophys. Res.*, *114*, E00D05, doi:10.1029/2009JE003343. [Printed *115*(E2), 2010].

Murchie, S. L., et al. (2009b), A synthesis of Martian aqueous mineralogy after 1 Mars year of observations from the Mars Reconnaissance Orbiter, *J. Geophys. Res.*, *114*, E00D06, doi:10.1029/2009JE003342. [Printed *115*(E2), 2010].

Murchie, S. L., et al. (2009c), Compact Reconnaissance Imaging Spectrometer for Mars investigation and data set from the Mars Reconnaissance Orbiter's primary science phase, *J. Geophys. Res.*, *114*, E00D07, doi:10.1029/2009JE003344. [Printed *115*(E2), 2010].

Neukum, G., et al. (2004), HRSC: The high resolution stereo camera of Mars Express, *Eur. Space Agency Spec. Publ.*, *ESA SP-1240*, 17–36.

Oelkers, E. H., and S. R. Gislason (2001), The mechanism, rates and consequences of basaltic glass dissolution: I. An experimental study of the dissolution rates of basaltic glass as a function of aqueous Al, Si and oxalic acid concentration at 25°C and pH = 3 and 11, *Geochim. Cosmochim. Acta*, *65*(21), 3671–3681, doi:10.1016/S0016-7037(01)00664-0.

Osterloo, M. M., et al. (2008), Chloride-bearing materials in the southern highlands of Mars, *Science*, *319*(5870), 1651–1654, doi:10.1126/science.1150690.

Pelkey, S. M., et al. (2007), CRISM multispectral summary products: Parameterizing mineral diversity on Mars from reflectance, *J. Geophys. Res.*, *112*, E08S14, doi:10.1029/2006JE002831.

Perkins, M. E., and B. P. Nash (2002), Explosive silicic volcanism of the Yellowstone hotspot: The ash fall tuff record, *Geol. Soc. Am. Bull.*, *114*(3), 367–381, doi:10.1130/0016-7606(2002)114<0367:ESVOTY>2.0.CO;2.

Perruchot, A., et al. (1997), L'halloysite karstique; comparaison des gisements types de Wallonie (Belgique) et du Perigord (France), *Clay Miner.*, *32*(2), 271–287, doi:10.1180/claymin.1997.032.2.08.

Plescia, J. B. (2004), Morphometric properties of Martian volcanoes, *J. Geophys. Res.*, *109*, E03003, doi:10.1029/2002JE002031.

Poulet, F., et al. (2005), Phyllosilicates on Mars and implications for early Martian climate, *Nature*, *438*(7068), 623–627, doi:10.1038/nature04274.

Poulet, F., et al. (2009), Quantitative compositional analysis of Martian mafic regions using the MEx/OMEGA reflectance data, *Icarus*, *201*(1), 69–83, doi:10.1016/j.icarus.2008.12.025.

Roach, L. H., et al. (2010), Hydrated mineral stratigraphy of Ius Chasma, Valles Marineris, *Icarus*, *206*(1), 253–268, doi:10.1016/j.icarus.2009.09.003.

Robinson, M. S., et al. (1993), Chronology, eruption duration, and atmospheric contribution of the Martian Volcano Apollinaris Patera, *Icarus*, *104*(2), 301–323, doi:10.1006/icar.1993.1103.

Schiffman, P., et al. (2000), Controls on palagonitization versus pedogenic weathering of basaltic tephra: Evidence from the consolidation and geochemistry of the Keanakako'i Ash Member, Kilauea Volcano, *Geochem. Geophys. Geosyst.*, *1*(8), 1040, doi:10.1029/2000GC000068.

Siever, R. (1962), Silica solubility, 0°–200°C., and the diagenesis of siliceous sediments, *J. Geol.*, *70*(2), 127–150, doi:10.1086/626804.

Silber, A., et al. (1994), Mineralogical and chemical composition of three tuffs from northern Israel, *Geoderma*, *63*(2), 123–144, doi:10.1016/0016-7061(94)90002-7.

Squyres, S. W., and J. F. Kasting (1994), Early Mars: How warm and how wet?, *Science*, *265*(5173), 744–749, doi:10.1126/science.265.5173.744.

Squyres, S. W., et al. (2006), Two years at Meridiani Planum: Results from the Opportunity Rover, *Science*, *313*(5792), 1403–1407, doi:10.1126/science.1130890.

Squyres, S. W., et al. (2008), Detection of silica-rich deposits on Mars, *Science*, *320*(5879), 1063–1067, doi:10.1126/science.1155429.

Swayze, G. A., et al. (2007), Spectral evidence for hydrated volcanic and/or impact glass on Mars with MRO CRISM, paper presented at Seventh International Conference on Mars, Lunar and Planet. Inst., Pasadena, Calif., 7–13 July.

Tanaka, K. L., and P. A. Davis (1988), Tectonic history of the Syria Planum Province of Mars, *J. Geophys. Res.*, *93*(B12), 14,893–14,917, doi:10.1029/JB093iB12p14893.

Thollot, P., et al. (2010), Recent hydrated minerals in Noctis Labyrinthus Chasmata, Mars, *Lunar Planet. Sci.*, *XLI*, Abstract 1873.

Tosca, N. J., et al. (2004), Acid-sulfate weathering of synthetic Martian basalt: The acid fog model revisited, *J. Geophys. Res.*, *109*, E05003, doi:10.1029/2003JE002218.

Wang, A., and Z. C. Ling (2011), Ferric sulfates on Mars: A combined mission data analysis of salty soils at Gusev crater and laboratory experimental investigations, *J. Geophys. Res.*, *116*, E00F17, doi:10.1029/2010JE003665.

Weitz, C. M., et al. (2010), Mineralogy and morphology of light-toned deposits in Noctis Labyrinthus, *Lunar Planet. Sci.*, *XLI*, Abstract 2240.

Weitz, C. M., et al. (2011), Diverse mineralogies in two troughs of Noctis Labyrinthus, Mars, *Geology*, *39*(10), 899–902, doi:10.1130/G32045.1.

Wendt, L., et al. (2011), Sulfates and iron oxides in Ophir Chasma, Mars, based on OMEGA and CRISM observations, *Icarus*, *213*(1), 86–103, doi:10.1016/j.icarus.2011.02.013.

Wray, J. J., et al. (2008), Compositional stratigraphy of clay-bearing layered deposits at Mawrth Vallis, Mars, *Geophys. Res. Lett.*, *35*, L12202, doi:10.1029/2008GL034385.

Wray, J. J., et al. (2011), Columbus crater and other possible groundwater-fed paleolakes of Terra Sirenum, Mars, *J. Geophys. Res.*, *116*, E01001, doi:10.1029/2010JE003694.

Ziegler, K., et al. (2003), Halloysite as a kinetically controlled end product of arid-zone basalt weathering, *Chem. Geol.*, *202*(3–4), 461–478, doi:10.1016/j.chemgeo.2002.06.001.

Zolotov, M. Y., and M. V. Mironenko (2007), Timing of acid weathering on Mars: A kinetic-thermodynamic assessment, *J. Geophys. Res.*, *112*, E07006, doi:10.1029/2006JE002882.

V. Ansan, S. Le Mouélic, N. Mangold, and P. Thollot, Laboratoire de Planétologie et Géodynamique, CNRS et Université de Nantes, UMR6112 2 rue de la Houssinière, BP 92205, F-44322 Nantes CEDEX 3, France. (patrick.thollot@univ-nantes.fr)

J. L. Bishop, Carl Sagan Center, SETI Institute, 189 N. Bernardo Ave., Mountain View, CA 94043, USA.

R. E. Milliken, Department of Civil Engineering and Geological Sciences, University of Notre Dame, 156 Fitzpatrick Hall, Notre Dame, IN 46556, USA.

S. L. Murchie, Johns Hopkins University Applied Physics Laboratory, 11100 Johns Hopkins Rd., Rm. MP3-W165, Laurel, MD 20723, USA.

J. F. Mustard, Department of Geological Sciences, Brown University, Box 1846, 324 Brook St., Providence, RI 02912, USA.

L. H. Roach, Frontier Technology, Inc., 100 Cummings Center, Ste. 450G, Beverly, MA 01915, USA.

C. M. Weitz, Planetary Science Institute, 1700 E. Fort Lowell Rd., Tucson, AZ 85719, USA.